

1 Cluster-based characterization of multi-dimensional tropospheric 2 ozone variability in coastal regions: an analysis of lidar 3 measurements and model results

4 Claudia Bernier¹, Yuxuan Wang¹, Guillaume Gronoff^{2,3}, Timothy Berkoff², K. Emma Knowland^{4,5}, John T.
5 Sullivan⁴, Ruben Delgado^{6,7}, Vanessa Caicedo^{6,7}, Brian Carroll^{2,6}

6 ¹Department of Earth and Atmospheric Science, University of Houston, Houston, Texas, USA

7 ²NASA Langley Research Center, Hampton, VA, 23666, USA

8 ³Science Systems and Application Inc., Hampton, VA, 23666, USA

9 ⁴NASA Goddard Space Flight Center, Global Modeling and Assimilation Office, Greenbelt, MD, 20771, USA

10 ⁵Morgan State University, Goddard Earth Science Technology & Research (GESTAR) II, Baltimore, Maryland, USA

11 ⁶Joint Center for Earth Systems Technology, Baltimore, MD, USA

12 ⁷University of Maryland Baltimore County, Baltimore, MD, USA

13 *Correspondence:* Yuxuan Wang (ywang246@central.uh.edu)

14

15 **Abstract.** Coastal regions are susceptible to multiple complex dynamic and chemical mechanisms and emission sources that
16 lead to frequently observed large tropospheric ozone variations. These large ozone variations occur on a meso-scale which
17 have proven to be arduous to simulate using chemical transport models (CTMs). We present a clustering analysis of multi-
18 dimensional measurements from ozone Light Detection And Ranging (LiDAR) in conjunction with both an offline GEOS-
19 Chem CTM simulation and the online GEOS-Chem simulation GEOS-CF, to investigate the vertical and temporal variability
20 of coastal ozone during three recent air quality campaigns: 2017 Ozone Water-Land Environmental Transition Study
21 (OWLETS)-1, 2018 OWLETS-2, and 2018 Long Island Sound Tropospheric Ozone Study (LISTOS). We developed and
22 tested a clustering method that resulted in 5 ozone profile curtain clusters. The established 5 clusters all varied significantly in
23 ozone magnitude vertically and temporally which allowed us to characterize the coastal ozone behavior. The lidar clusters
24 provided a simplified way to evaluate the two CTMs for their performance of diverse coastal ozone cases. ~~The two models~~
25 ~~have fair to good relationships with the lidar observations ($R = 0.66$ to 0.69) in the low-level altitude range (0 to 2000 m),~~
26 ~~with low and unsystematic bias for GEOS-Chem and high systemically positive bias for GEOS-CF. In the mid-level altitude~~
27 ~~range (2000 to 4000 m), both models have difficulty simulating the vertical extent and variability of ozone concentrations in~~
28 ~~all 5 clusters, with a weak relationship with the lidar observations ($R = 0.12$ and 0.22 , respectively). GEOS-Chem revealed a~~
29 ~~high systematic negative bias and GEOS-CF an overall low unsystematic bias range. Using ozone vertical and diurnal~~
30 ~~distribution from lidar measurements, this work provides new insights on model's proficiency in complex coastal regions. An~~
31 ~~overall evaluation of the models reveals good agreement ($R \approx 0.70$) in the low-level altitude range (0 to 2000 m), with a low~~

32 and unsystematic bias for GEOS-Chem and high systemic positive bias for GEOS-CF. The mid-level (2000 – 4000 m)
33 performances show a high systematic negative bias for GEOS-Chem and an overall low unsystematic bias for GEOS-CF and
34 a generally weak agreement to the lidar observations (R = 0.12 and 0.22, respectively). In evaluating the cluster specific
35 performances additional model insight is revealed as cluster-by-cluster model performance is more convoluted than the overall
36 performances suggest. Utilizing the full vertical and diurnal ozone distribution information specific to lidar measurements, this
37 work provides new insights on model’s proficiency in complex coastal regions.

38

39 **1. Introduction**

40 Tropospheric ozone (O₃) is an important secondary pollutant created by multiple reactions involving sunlight, nitrogen
41 oxides (NO_x = NO + NO₂), and volatile organic compounds (VOCs) which, in accumulation, can have damaging effects on
42 human and plant health. In addition to its photochemical growth, O₃ can easily be influenced by local and regional transport
43 mechanisms. For coastal regions, surface O₃ is highly variable in time and space due to its susceptibility to many factors such
44 as local ship emissions, long range transport, and sea/bay breeze processes. Multiple studies have proven the strong influence
45 that sea/bay breeze and wind flow patterns can have on the accumulation of coastal O₃ and can often lead to poor air quality
46 (e.g., Tucker et al., 2010; Martins et al., 2012; Stauffer et al., 2012; Li et al., 2020). Loughner et al. (2014) highlighted the
47 importance for understanding the ability for bay breeze events to cause O₃ differences not only spatially but vertically in coastal
48 regions.

49 This variability is challenging for air quality models to capture as high-resolution measurements are necessary to fully
50 understand and simulate this O₃ behavior in coastal regions. For example, Dreessen et al. (2019) tested the U.S. Environmental
51 Protection Agency (EPA) Community Multiscale Air Quality (CMAQ) model’s ability, configured at 12 km, to simulate O₃
52 exceedances at Hart Miller Island in Maryland (HMI) revealing high bias and ‘false alarms’ due to several reasons such as
53 emission transport over water and the coarse model resolution’s inability to capture fine-scale meteorology and transport.
54 Cases such as sea/bay breeze events, which directly contribute to high coastal O₃ cases, are denoted by local meteorological
55 mechanisms such as surface wind speed deceleration, wind direction convergence and recirculation (Banta et al., 2005). Air
56 quality models with coarse horizontal and vertical resolutions are not able to capture such fine developments (Caicedo et al.,
57 2019). Ring et al. (2018) also used CMAQ to estimate the impact of ship emissions on the air quality in eastern U.S. coastal
58 regions indicating that an understanding of the vertical profiles of emissions was significant for improving air quality
59 simulations. These are consistent and unanimous issues with air quality modeling in coastal regions. Since offshore sites within
60 coastal regions are historically under sampled due to the difficulty of water-based measurements, this problem is still pertinent
61 today.

62 Recently, three associated air quality campaigns set out to address this issue (<https://www-air.larc.nasa.gov/index.html>):
63 2017 & 2018 NASA Ozone Water-Land Environmental Transition Study (OWLETS-1 & OWLETS-2) and Long Island Sound
64 Tropospheric Ozone Study (LISTOS), ~~set out to address this issue~~ (e.g., Sullivan et al., 2019). These three campaigns were
65 each conducted in highly populated coastal regions along the Chesapeake Bay in Virginia and Maryland and Long Island

66 Sound in the New England/Middle Atlantic region, respectively, that are vulnerable to O₃ exceedances with the goal of filling
67 the measurement gaps in these regions. During these campaigns, a suite of detailed airborne and ground measurements were
68 taken during the course of highly polluted summer months (end of May through August) to capture the variability of pollutants,
69 including O₃ and its precursor species, and the distinct meteorological processes specific to land-water regions that affect them.

70 The three campaigns strategically placed multi-dimensional tropospheric lidar measurements of O₃ on and offshore in
71 order to capture critical land-water gradients and to fill the deficit of measurements in these under monitored areas. These
72 measurements were supported as part of NASA's Tropospheric Ozone Lidar Network (TOLNet). Continuous profile
73 measurements from O₃ lidars highlight important regional transport and temporal variations of O₃ in the lower and middle
74 levels of the troposphere that are usually difficult to capture by most satellite-based remote-sensing instruments (Thompson et
75 al., 2014). Lidar measurements are unique in their ability to capture high resolution full O₃ 2-D profile curtains over a period
76 of time that indicate pollutant transport and can help in understanding O₃ behavior in coastal regions. In Gronoff et al. (2019),
77 the co-located lidar at the Chesapeake Bay Tunnel Bridge (CBBT) during OWLETS-1 successfully captured a near-surface
78 maritime ship plume emission event on August 01, 2017. An ensemble of other instruments (e.g., drones, Pandora spectrometer
79 systems, etc.) launched near the shipping channel captured elevated NO₂ concentrations while the lidar instrument captured a
80 depletion of O₃ simultaneously. The lidar was able to capture the unique low range altitude O₃ concentrations which elucidated
81 the evolution of the trace-gas concentrations during this ship plume event.

82 Several studies have thoroughly evaluated the results from the air quality campaigns used in this study but were focused
83 more on specific case studies (Dacic et al., 2019; Sullivan et al., 2019; Gronoff et al., 2019). Dacic et al. (2019) used lidar
84 measurements of a high O₃ episode during OWLETS-1 to evaluate the ability of two NASA coupled chemistry-meteorology
85 models (CCMMs), the GEOS Composition Forecast ("GEOS-CF"; Keller et al., 2021) and MERRA2-GMI (Strode et al.,
86 2019), to simulate this high O₃ event. They found that the GEOS-CF model performed fairly in simulating O₃ in the lower
87 level (between 400 to 2000 m ASL) and outperformed MERRA2-GMI based on surface observations at multiple monitoring
88 sites and by a median difference of -6 to 8 % +/- 7 % at both lidar sites. In the case of this event, GEOS-CF was able to simulate
89 the 2-D O₃ profile curtains at small scales. At the time of the Dacic et al. (2019) study, only processed observational data from
90 OWLETS-1 was available.

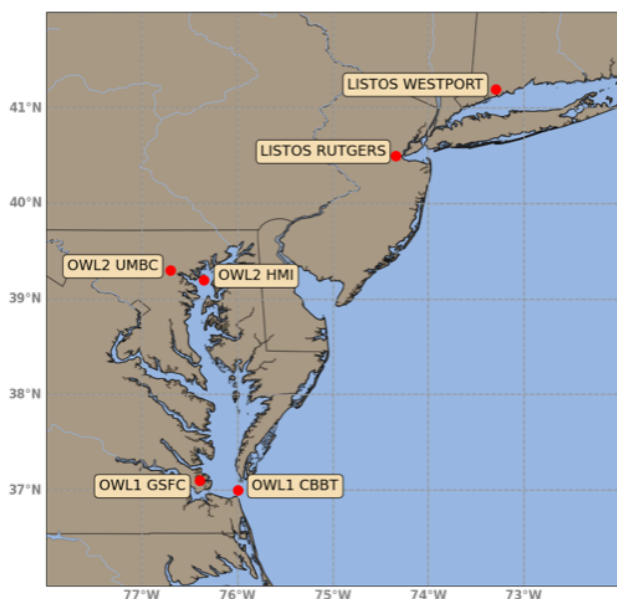
91 For this study, we took advantage of 91 captured 2-D (vertical and diurnal) O₃ profile curtains from all three air quality
92 campaigns (Sect. 2). To characterize the different behaviors of O₃ in coastal regions, we developed a novel clustering method
93 based on the altitude and time dimensions of the lidar measurements that organized the profile curtains (Sect. 2). We used the
94 developed clusters to evaluate the ability of both offline and online GEOS-Chem and GEOS-CF simulations to reproduce the
95 coastal O₃ and wind characteristics highlighted by each cluster (Sect. 3).

96

97 **2. Materials & Method**

98 **2.1. Air quality campaigns**

99 During the years 2017 and 2018, NASA in partnership with other U.S. national agencies and university research groups
100 orchestrated three air quality campaign studies that focused on key land and water observations: OWLETS-1, OWLETS-2,
101 and LISTOS. OWLETS-1 was conducted in 2017 from July 5 to August 3, while OWLETS-2 and LISTOS were conducted in
102 2018 from June 6 to July 6 and July 12 to August 29, respectively. All campaigns took advantage of a multitude of ground,
103 aircraft, and remote sensing measurements. For the sake of this study, we will focus on measurements from the two lidars from
104 the TOLNet: NASA Langley Mobile Ozone Lidar (LMOL) (De Young et al. 2017; Farris et al. 2018; Gronoff et al, 2019,
105 2021) and NASA Goddard Space Flight Center (GSFC) Tropospheric Ozone (TROPOZ) Differential Absorption Lidar (DIAL)
106 (Sullivan et al. 2014, 2015a), which ran simultaneously at the marked positions in Figure 1. The TOLNet data from all three
107 campaigns are available on the NASA LaRC Airborne Science Data for Atmospheric Composition archive ([https://www-
108 air.larc.nasa.gov/missions.htm](https://www-air.larc.nasa.gov/missions.htm); accessed – 20 January 2021).
109



110 **Figure 1.** An inset map of the Chesapeake Bay airshed in Maryland, Virginia, and Long Island Sound in New York with the
111 six lidar monitoring locations used for OWLETS-1, OWLETS-2, and LISTOS highlighted and labeled.

112 The two lidars were placed strategically for each campaign (Figure 1), so that one lidar was closest to over-water
113 measurements while the other was farther inland with the goal of examining how O_3 transport and concentration is influenced
114 by specific coastal mechanisms such as the land–water breezes. For OWLETS-1, the LMOL lidar was used at the CBBT
115 [37.0366°N, 76.0767°W], depicting the real time over water O_3 measurements while the GSFC TROPOZ lidar was stationed
116 at NASA Langley Center [37.1024°N, 76.3929°W] further inland. Similarly, for OWLETS-2, the LMOL lidar was stationed
117 for the over water measurements at Hart Miller Island [39.2449° N, 76.3583° W] and GSFC TROPOZ was stationed at the

118 University of Maryland, Baltimore County (UMBC) [39.2557° N, 76.7111° W]. Finally, for LISTOS, LMOL was at the
119 Westport site [41.1415° N, 73.3579° W] and TROPOZ at Rutgers [40.2823° N, 74.2525° W]. For the sake of this study the
120 unique benefits due to the different placements (onshore versus offshore) of the co-located lidars are not specifically evaluated.
121 Instead, the study focuses on the benefits of detailed and multi-dimensionality of both lidar instrument data in general.

122 Routine lidar measurements were taken for the duration of the campaigns providing 91 multi-dimensional O₃ profile
123 curtains. Both lidars retrieve data at a 5-min temporal resolution and use a common processing scheme to produce a final O₃
124 product which was used for this study. In this study, the individual profile curtains refer to the “full day”, vertical and diurnal
125 lidar measurements. In this study, 91 individual 2-D profile curtains were used from both lidars from the three campaigns: 26
126 profile curtains from OWLETS-1, 28 profile curtains from OWLETS-2, and 37 profile curtains from LISTOS.

127 To evaluate meteorological impacts on the lidar O₃ clusters and distinguish certain model discrepancies we used various
128 temperature and wind measurements. Hourly observed temperature, wind speed, and wind direction, and O₃ from surface
129 monitors pertaining to the study area were obtained from the Air Quality System (AQS) (data can be accessed at
130 <https://aqs.epa.gov/aqsweb/airdata/>). Along with the O₃ lidar instruments, we utilized high resolution vertical and horizontal
131 wind speed and direction data monitored by Doppler wind lidar Leosphere WINDCUBE 200s instruments deployed at HMI
132 during OWLETS-2 during LISTOS (e.g., Couillard et al., 2021; Coggon et al., 2021; Wu et al., 2021).

133

134 **2.2. Clustering lidar data**

135 **2.2.1 Description of the ozone lidar measurements**

136 The lidar instrument is unique in that it provides high dimensional profile measurements of O₃, as opposed to one
137 dimensional surface measurements from air quality monitoring sites. The two TOLNet lidars used during the campaigns have
138 been evaluated for their accuracy during previous air quality campaigns (DISCOVER-AQ; [https://www-](https://www-air.larc.nasa.gov/missions/discover-aq)
139 [air.larc.nasa.gov/missions/discover-aq](https://www-air.larc.nasa.gov/missions/discover-aq) and FRAPPÉ; <https://www2.acom.ucar.edu/frappe>) and have also been compared
140 against each other (e.g., Sullivan et al., 2015; Wang et al., 2017). The two lidars have different transmitter and retrieval
141 components but produce O₃ profiles within 10 % of each other as well as compared to ozonesondes (Sullivan et al., 2015). In
142 comparison with other in situ instrument measurements, the TOLNet lidars were found to have an accuracy better than ±15 %
143 for capturing high temporal tropospheric O₃ vertically proving their capability of capturing high temporal tropospheric O₃
144 variability (Wang et al., 2017; Leblanc et al., 2018).

145 To characterize coastal O₃ during the summer months, we use a multitude of lidar profile curtains obtained during the
146 OWLETS-1, 2, and LISTOS campaigns. The two lidars used in the campaigns produced profile curtains of O₃ from 0 – 6000
147 m above ground level (AGL) with some days beginning as early as 06:00 local time (EDT) and ending measurements as late
148 as the last hour of the day. One of the challenges is that the multiple lidar datasets are not always uniform; although most of
149 the profile curtains began at or around 08:00 EDT, the lidar measurements commence and conclude at different times. At the
150 time of these campaigns, the lidar data retrieval was constrained by the availability of personnel as well as the availability of
151 electricity in remote areas (at time of writing, the lidar instrument systems have been updated and are now more fully

152 automatized for use during succeeding campaigns removing such constraints). Due to this constraint, the 91 lidar curtains
153 range from as short as a 6-hour window to a full 24-hour window. Similarly, the profile curtains do not have an exact uniform
154 altitude range either. In the processing of the lidar data, some measurements may be filtered out and removed due to issues,
155 such as clouds, which can influence and degrade the retrieval leaving some blocks of empty data within the vertical altitude
156 dimension. When the cloud conditions are perfect, the limiting factor for the altitude is the solar background: the UV from the
157 sun is a source of noise that prevents the detection of the low level of backscattered photons. For LMOL, this means that the
158 maximum altitude is about 10 km AGL at night (Gronoff et al., 2021) and lowered to about 4 km AGL at solar noon (worse
159 conditions possible for the summer in the continental U.S. resulting in below 4 km AGL). This results in a general scarcity of
160 O₃ measurements above 4000 m AGL for most of the vertical profile curtains. Lidars still have limitations that prove to be a
161 complication e.g., noise signal and manual operations. At the time of writing, the operative limitation has been addressed and
162 the lidars are now more fully automated which removes some of the difficulty.

163

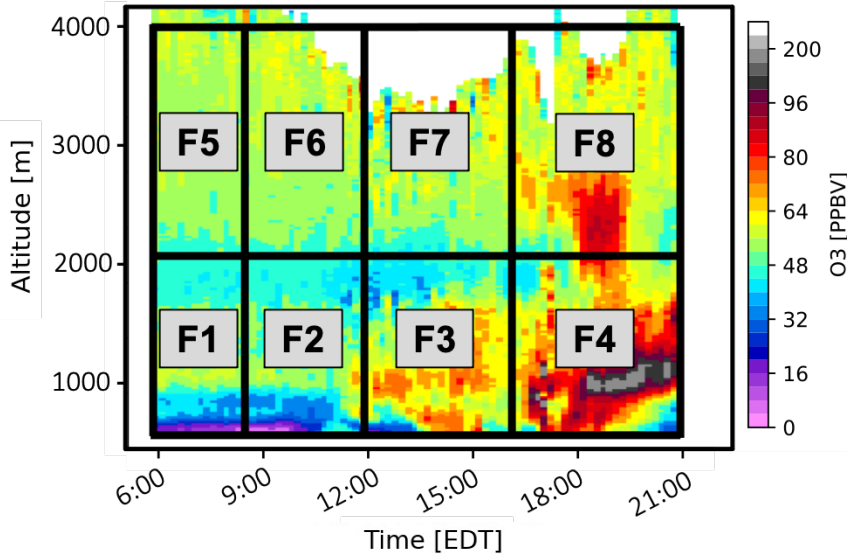
164 2.2.2 Clustering approach and application

165 To facilitate the comparison of the 2-D O₃ profile curtains and the air quality model simulations we used a cluster analysis
166 that categorized the behavior of the tropospheric O₃ captured in the profile curtains. Clustering methods are commonly used
167 in air quality and atmospheric studies to group and characterize large datasets (Darby, 2005; Alonso et al., 2006; Christiansen,
168 2007; Davis et al., 2010; Stauffer et al., 2018). In our previous work, we have successfully used clustering methods to
169 automatically characterize diurnal patterns of surface winds and surface O₃ in the Houston-Galveston-Brazoria area that proved
170 to perform better than a rudimentary quantile method to reveal the dependence of surface O₃ variability on local and synoptic
171 circulation patterns on the Gulf Coast (Bernier et al., 2019; Li et al., 2020)

172 In evaluating the structure of the lidar measurements and working within measurement limitations (described in Sect.
173 2.2.1) from the three air quality campaigns, we developed a method to cluster multi-dimensional O₃ profile curtains using K-
174 Means clustering algorithm. Input features (seed values) were rationally established to best represent the behavior of O₃
175 temporally and vertically without including an excessive amount of input features, which can weaken the results of clustering
176 (discussed in detail in Sect. S1). With the goal of evaluating lower level tropospheric O₃ and based on description of the
177 structure and constraints of the lidar measurements, the features were tailored to the altitude range 0 – 4000 m AGL and time
178 range of 06:00 EDT – 21:00 EDT.

179 Figure 2 illustrates the 8 features that represent slabs of altitude and time used in the cluster analysis. For each O₃ profile
180 curtain (total of 91), we calculated the average O₃ from the following time and altitude range: Features 1 – 4 altitudes range
181 from 0 – 2000 m; Features 5 – 8 altitudes range from 2000 – 4000 m. The two altitude ranges were determined to best represent
182 different O₃ transport events although they do not explicitly represent these layers. For Features 1 – 4, O₃ would most likely
183 primarily be affected by local production and pollution transport while for Features 5 – 8, O₃ would more likely be associated
184 with long range transport (e.g. interstate). As planetary boundary layer growth (PBL) in coastal regions do not usually reach
185 altitudes greater than 2000 m, mixing between the boundary layer and free troposphere would presumably take place within

186 the low-level altitude bin. Additional attention to the PBL in the selecting of low versus mid-level features for the clustering
187 will be investigated in future work. For clarity, we will use the terms low-level and mid-level features to address the two
188 altitude subsets e.g., Features 1 – 4 and 5 – 8, respectively. Feature 1 and 5 time range from 06:00 – 08:00 EDT; Feature 2 and
189 6 from 08:00 – 12:00 EDT; Feature 3 and 7 from 12:00 – 16:00 EDT; and Feature 4 and 8 from 16:00 – 21:00 EDT. The four
190 subset time ranges were indicated to best represent features that characterize the common diurnal behavior of O₃.



191
192 **Figure 2.** Clustering method developed for clustering vertical O₃ profiles taken from lidar measurements. The color coding
193 shows a typical day of lidar measurements of O₃ profiles on August 6, 2018, from the LMOL at Westport, CT during the
194 LISTOS Campaign. F1 – F8 indicate the time and altitude range of the eight features used for the clustering algorithm.

195
196 The features were evaluated for cluster tendency, essentially to confirm our dataset contained meaningful clusters
197 [\(discussed in detail in Sect. S2\)](#). One statistical approach was used to test the dataset called Hopkins statistic which measures
198 whether there is uniform distribution (spatial randomness) within the dataset (Lawson and Jurs, 1990). The results calculated
199 using the Hopkins statistic concluded a value higher than 0.75 (actual = 0.77) which by this standard indicates a clustering
200 tendency at the 90 % confidence level. Evaluating different feature options did not lead to better statistical results than with
201 the final chosen features. To visualize the cluster tendency of our dataset, we applied the algorithm of the visual assessment of
202 cluster tendency (VAT) approach (Bezdek and Hathaway, 2002) which uses the Euclidean distance measure to compute the
203 dissimilarity matrix in the dataset and creates an ordered dissimilarity matrix image. Figure S1 shows the VAT approach results
204 which indicates high similarity (red) and low similarity (blue) and confirms a cluster structure (not random) within our dataset.

205 Since the choice of clustering algorithm is subjective, we chose K-means clustering for its simplicity and widespread use.
206 To use the K-Means clustering algorithm, the optimal number of clusters based on your dataset must be chosen beforehand.
207 For this study, the package Nbclust (Charrad et al., 2014) in R was used, which applies 30 indices for determining the optimal

208 number of clusters. Using this package, as well as testing the quality of the clustering results using the silhouette method
209 (Kaufman & Rousseeuw, 1990), we selected six clusters as the optimal number of clusters. Since the K-Means clustering
210 algorithm is based on the Euclidean distance to each centroid, the input data was normalized (to a mean of zero and standard
211 deviation of one) to ensure each feature is given the same importance in the clustering (Aksoy & Haralick, 2001; Larose,
212 2005). The resulting six clusters (described fully in Sect. 3.1) represent clusters of regularly observed lidar O₃ curtains for the
213 regions of our study during the campaign periods.

214

215 **2.2.3 Missing data**

216 Although the input features were tailored based on the structure of the lidar measurements, the remaining data still had
217 missing data points. In performing a quick evaluation on the 8 input features (Figure S54), we found that Features 1, 4, 5, and
218 8 had the most missing data while Features 2, 3, 6, and 7 had few or zero cases of missing data. This means that the earlier
219 morning measurements (06:00 – 12:00 EDT) and the later evening measurements (16:00 – 21:00 EDT) had the most cases of
220 missing data points. This is plausible as the campaign teams were best able to retrieve clear measurement during
221 midday/evening hours (12:00 – 16:00 EDT). As a result, 51 out of 91 O₃ profile curtains had at least one missing data point
222 (feature) throughout the individual profile curtain.

223 A common practice for dealing with missing data is complete case analysis (CCA), in which observations with missing
224 values are completely ignored, leaving only the complete data to cluster. CCA can be inefficient as it introduces selection bias
225 since the sample data no longer retains the state of the original full dataset (Donders et al., 2006; Little & Rubin, 2014). When
226 we applied CCA, there were only 40 O₃ profile curtains of complete data, removing over half of the study profiles. Instead,
227 we used a more comprehensive solution – imputation - that yields unbiased results (Donders et al., 2006). For this study we
228 used the single imputation (SI) technique *knnImputation* in R (Torgo, 2010), which uses the k-nearest neighbors and searches
229 for the most similar cases and uses the weighted average of the values of those neighbors to fill the missing data. Essentially,
230 this method selects the days that have the most similar profile curtain to any profile which has missing data points and uses
231 those real data points to calculate a weighted mean that will fill in the missing data. We acknowledge using an imputation
232 method on the dataset will possibly introduce a bias which is difficult to quantify, but this allows the use of the full 91 profile
233 curtains of O₃ data. The silhouette method was used to test the quality of the newly imputed dataset and proved to be no worse,
234 nor better, than the CCA (*real data*) results. Therefore, the dataset was first imputed using SI to create a complete dataset and
235 then the clustering method described in the sect. before (2.2.2) was applied to the complete imputed dataset.

236

237 **2.3. Model simulations**

238 The offline GEOS-Chem chemical-transport model (CTM) was utilized to simulate the spatial and temporal variability
239 of coastal O₃ in the Chesapeake Bay and Long Island Sound during the time of the campaigns. The GEOS-Chem model is a
240 global 3-D CTM driven by assimilated meteorological data from the NASA Global Modeling and Assimilation Office
241 (GMAO). Our simulations were driven by reanalysis data from Modern-Era Retrospective analysis for Research and

242 Applications, Version 2 (MERRA-2; Gelaro et al., 2017). We ran a nested GEOS-Chem (v12-09) simulation at $0.5^\circ \times 0.625^\circ$
243 horizontal resolution over the eastern portion of North America and adjacent ocean ($90 - 60^\circ\text{W}$, $20 - 50^\circ\text{N}$), using lateral
244 boundary conditions updated every three hours from a global simulation with $2^\circ \times 2.5^\circ$ horizontal resolution. The nested
245 GEOS-Chem simulation was run with 72 vertical levels from 1013 to 0.01 hPa. Since the study focuses on the altitude range
246 $0 - 4000$ m, the first 20 vertical levels from GEOS-Chem were used with 14 levels within the boundary layer (≤ 2000 m). The
247 nested simulation was conducted for the study periods June – September 2017 and April – August 2018. We used the standard
248 “out-of-the-box” unmodified default settings from the tropospheric chemistry chemical mechanism (tropchem) with global
249 anthropogenic emissions from the Community Emissions Data System (CEDS) inventory (McDuffie et al, 2020) and U.S.
250 Environmental Protection Agency (EPA) National Emissions Inventory (NEI) 2011 for monthly mean North American
251 regional emissions (EPA NEI, 2015).

252 We also used results from NASA’s near real-time forecasting system, GEOS-CF, an online GEOS-Chem simulation (v12-
253 0-1) from GMAO (https://gmao.gsfc.nasa.gov/-weather_prediction/GEOS-CF/) with GEOS coupled to the GEOS-Chem
254 tropospheric-stratospheric unified chemistry extension (UCX) and run at a high spatial resolution of 0.25° , roughly 25 km
255 (Keller et al., 2021, Knowland et al., 2021). The vertical resolution for GEOS-CF is interpolated onto 72 vertical levels from
256 1000 to 10 hPa. Since the study focuses on the altitude range $0 - 4000$ m, the first 21 vertical levels from GEOS-CF were used
257 with 14 levels within the boundary layer (≤ 2000 m). Prior to the launch of the 12z five-day forecast, GEOS-CF produces daily
258 global, 3-D atmospheric composition distributions using the GEOS meteorological replay technique (Orbe et al., 2017), and
259 this study makes use of these historical estimates, made available to the public for the period since January 2018. Therefore,
260 the GEOS-CF results shown in this study only include the dates from OWLETS-2 and LISTOS campaigns, since they both
261 occurred in 2018.

262 While both model simulations use similar versions of GEOS-Chem chemistry, there are noteworthy differences to keep
263 in mind during the analysis of the clustering. The main differences between the two models are (1) GEOS-Chem is an offline
264 CTM using archived meteorology, while GEOS-CF simulates atmospheric composition simultaneously with meteorology
265 (online); (2) the spatial resolution of the GEOS-CF model (0.25°) is higher than GEOS-Chem ($0.5^\circ \times 0.625^\circ$); and (3) the
266 GEOS-CF model runs with Harmonized Gridded Air Pollution (HTAP; v2.2; base year 2010) anthropogenic emissions from
267 the Emission Database for Global Atmospheric Research (EDGAR), while GEOS-Chem was run with CEDS anthropogenic
268 emissions (base year 2014). These imperative differences can lead to disparities in the following results.

269

270 **3. Results & Discussion**

271 **3.1 Overview of the 2-D O₃ curtain clusters**

272 The clustering results reveal distinctive characterized O₃ behavior during the three campaigns in which O₃ concentrations
273 vary ~~significantly~~ across the clusters. As previously mentioned in Sect. 2.2.3, the clustering analysis initially identified six
274 cluster groups from the O₃ profile curtains. Only one date was assigned to Cluster 6 (16 June 2018): the lidar profile curtain
275 on this day (Figure S63) shows a large fraction of data missing, and the available data have relatively high O₃ throughout the

276 lowest 3 km, which is different from other clusters. Therefore, we consider Cluster 6 to be an outlier and will not include it in
 277 the subsequent analysis.

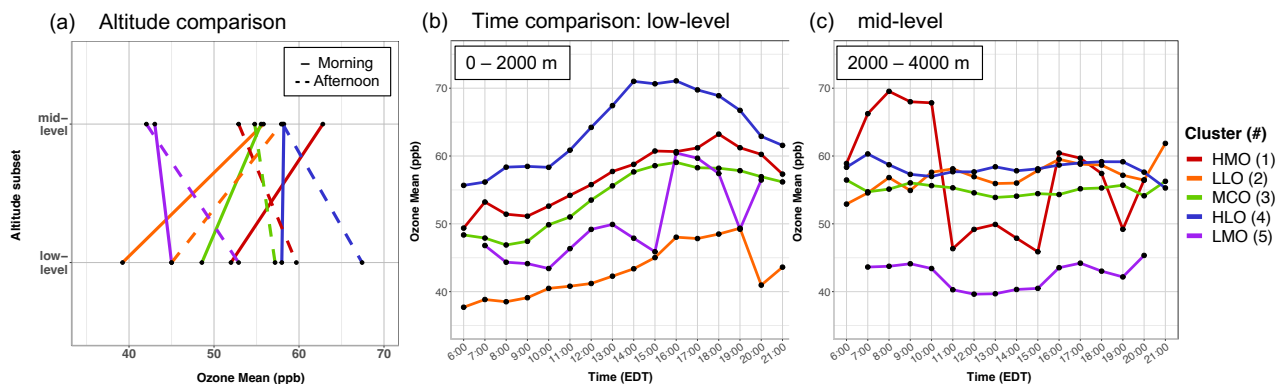
278 Various O₃ and surface meteorological parameter cluster statistics for the remaining five clusters are summarized in Table
 279 1. With only 5 of the 2-D profile curtains assigned, Cluster 5 depicts the least common O₃ behavior during the campaigns. On
 280 the other hand, Cluster 3 is the most common O₃ behavior during the campaigns with 28 profile curtains assigned to this
 281 cluster. Following Cluster 3, Cluster 1 is the next most common cluster with 25 profile curtains. Cluster 2 and Cluster 4 fall in
 282 the middle with 14 and 18 profile curtains assigned to the cluster numbers, respectively.

<u>Cluster #</u>	<u>a) No. of vertical profiles</u>	<u>b) O₃ Max (ppb)</u>	<u>c) O₃ Min (ppb)</u>	<u>d) T avg. (min; max) (°F)</u>	<u>e) WS avg. (min; max) (m s⁻¹)</u>
<u>1</u>	<u>25</u>	<u>86.5</u>	<u>42.2</u>	<u>74.1 (67.8; 86.4)</u>	<u>1.5 (0.5; 2.8)</u>
<u>2</u>	<u>14</u>	<u>72.8</u>	<u>28.9</u>	<u>71.6 (64.0; 83.9)</u>	<u>1.6 (0.6; 2.9)</u>
<u>3</u>	<u>28</u>	<u>86.6</u>	<u>34.2</u>	<u>77.2 (67.0; 87.6)</u>	<u>1.3 (0.5; 2.4)</u>
<u>4</u>	<u>18</u>	<u>97.8</u>	<u>44.1</u>	<u>78.4 (68.0; 90.4)</u>	<u>1.2 (0.4; 2.3)</u>
<u>5</u>	<u>5</u>	<u>67.7</u>	<u>29.1</u>	<u>74.5 (66.8; 74.5)</u>	<u>1.2 (0.3; 3.4)</u>

292 **Table 1.** Lidar vertical O₃ profile cluster statistics: a) total number of vertical profiles; b) O₃ maximum; c) O₃ minimum O₃;
 293 AQS monitoring station cluster mean d) surface temperature and e) wind speed; minimum and maximums in parenthesis. The
 294 statistics and averages were derived from the total number of profile curtains assigned to each cluster.

295
 296 The five clusters were distinguished by the varying O₃ concentrations between the low-level and mid-level as well as
 297 ~~temporal~~ diurnal variations (Figure 3). Figure 3a quantifies the between-cluster differences. We separate the data by the two
 298 altitude subsets (low and mid-level) and by two time subsets (morning = 6:00 – 12:00 and afternoon = 12:00 – 21:00) for
 299 lucidity as the majority of the cluster differences are contrasted between these subsets. In the low-level, all five clusters exhibit
 300 the common O₃ diurnal pattern where surface O₃ is titrated overnight and reaches a minimum but then is quickly exacerbated
 301 with the increase of sunlight throughout the day and typically peaks after midday (Figure 3b). The extent of this common
 302 diurnal pattern varies by cluster.

303



304

305 **Figure 3.** Lidar O₃ cluster average comparisons (five clusters depicted in colors). a) Altitude comparison of mean O₃ averaged
 306 over time: morning hours from 6:00 – 12:00 (solid line) and afternoon hours from 12:00 – 21:00 (dashed lines). Time
 307 comparison of mean hourly O₃ split between the b) low-level and c) mid-level.

308

309 ~~Cluster 1 has the second highest low level O₃ peak and the highest mid level O₃ concentrations averaging at 67 ppb~~
 310 ~~(Figure 3a). Cluster 1 also exhibit the most unique pattern of mid level O₃ (Figure 3c), with the highest concentrations found~~
 311 ~~in the early morning and an uncharacteristic plunge to lower O₃ concentrations from 11:00 – 15:00 EDT. This is contrary to~~
 312 ~~the other clusters which do not show as much O₃ magnitude variation temporally in the mid level. In assessing the individual~~
 313 ~~curtain profiles assigned to Cluster 1, the majority of the curtains reveal concentrated residual layers in the mid level and early~~
 314 ~~in the temporal profile that diffuse after the morning. This explains the uncharacteristic behavior of mid level O₃ in Cluster 1.~~
 315 ~~Cluster 2 has the lowest low level O₃ peak among the clusters averaging at 44 ppb (Figure 3a) with also the lowest morning~~
 316 ~~O₃ (from 6:00 – 10:00 EDT) and moderate mid level O₃ concentrations. Distinct from the other clusters that differ greatly in~~
 317 ~~O₃ concentrations vertically, Cluster 3 has the most uniform vertical O₃ extent between the low and mid level (Figure 3a).~~
 318 ~~Cluster 4 reaches the highest low level O₃ concentrations, averaging at 64 ppb (Figure 3a) and reaching > 70 ppb temporally~~
 319 ~~(Figure 3b). Finally, Cluster 5 has, considerably, the lowest mid level O₃ (Figure 3c) averaging at 45 ppb (Figure 3a), almost~~
 320 ~~40 ppb lower than the other clusters. Cluster 5 also has the most variable low level O₃ diurnal pattern (Figure 3b) which could~~
 321 ~~be attributed to the averaging of only five different profile curtains that were assigned to this cluster (Table 1).~~

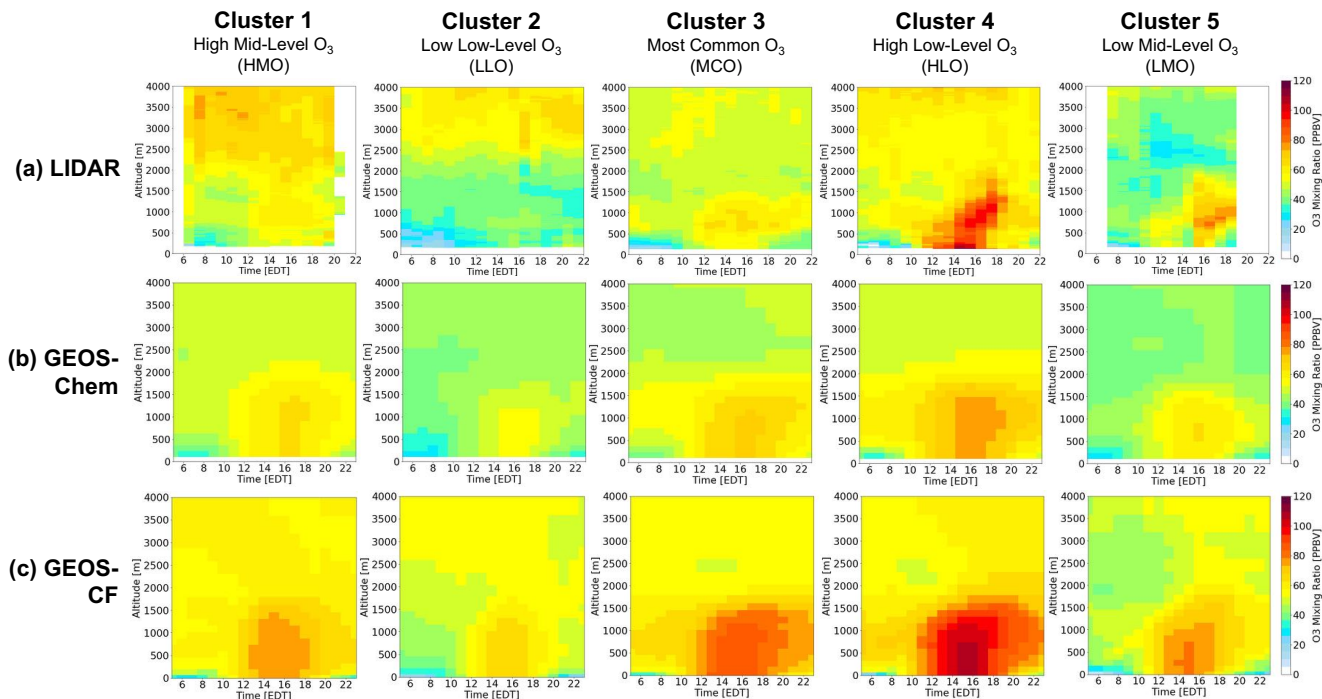
322 Cluster 1 in the low-level has the second highest morning and afternoon O₃ average (52 and 59 ppb) and in the mid-level
 323 the highest morning O₃ average (64 ppb) (Figure 3a). Cluster 1 also exhibits the most unique pattern of mid-level O₃ (Figure
 324 3c), with the highest concentrations found in the early morning and an uncharacteristic plunge to lower O₃ concentrations from
 325 11:00 – 15:00 EDT. This is contrary to the other clusters which do not show much O₃ variation temporally in the mid-level.
 326 The majority of the individual profile curtains assigned to Cluster 1 show concentrated early morning residual layers in the
 327 mid-level that diffuse after the morning, which is distinctive to the other clusters. In the low-level, Cluster 2 has the lowest
 328 morning and afternoon O₃ average among the clusters (39 and 45 ppb) with moderate mid-level O₃ concentrations. Cluster 3
 329 has the most uniform vertical O₃ extent between the low and mid-level (Figure 3a), in contrast to the other clusters that differ

330 greatly in O₃ concentrations between the two altitude subsets. Cluster 4 has the highest morning and afternoon O₃ averages (59
 331 and 68 ppb) in the low-level, reaching > 70 ppb temporally (Figure 3b). Finally, Cluster 5 has, considerably, the lowest morning
 332 and afternoon O₃ averages (42 and 43 ppb) in the mid-level, almost 10 ppb lower than the other clusters. Cluster 5 does not
 333 have a smooth-evolving O₃ diurnal pattern in the lower level (Figure 3b), which can be attributed to the averaging of only five
 334 different profile curtains that were assigned to this cluster (Table 1).

335 Figure 4a illustrates the mean lidar O₃ 2-D profile curtains for each of the clusters. For Cluster 1, 3, 4, and 5, higher O₃
 336 concentrations in the low-level are captured during afternoon/evening time (12:00 – 21:00 EDT), with the highest low-level
 337 O₃ in Cluster 4 (> 70 ppb). This behavior follows the common diurnal pattern of O₃, that was distinguishable in Figure 3b. This
 338 common O₃ growth reaches vertically to approximately 1500 m for each of the clusters but is generally contained below 2000
 339 m. Differing from the low-level O₃ behavior, mid-level O₃ is generally less variable in magnitude throughout the entire profile
 340 curtain (except for Cluster 1; see Figure 3a). The highest O₃ concentrations for the mid-level are exhibited in Cluster 1, 2, 3,
 341 and 4, with the highest mid-level O₃ in Cluster 1 during the early morning hours (≥ 70 ppb).

342 Following the descriptions above, each cluster is given a nomenclature according to their unique characteristics. Cluster
 343 1 is termed as the highest mid-level O₃ (HMO) cluster; Cluster 2 as the lowest low-level O₃ (LLO) cluster; Cluster 3 is the
 344 most common O₃ (MCO) cluster; Cluster 4 is the highest low-level O₃ (HLO); Cluster 5 is the least common and lowest mid-
 345 level O₃ (LMO) cluster. The O₃ variability represented and justified above is what led to the successful clustering of the lidar
 346 O₃ 2-D profile curtains.

347



348

349 **Figure 4.** Cluster-mean O₃ vertical profile results by cluster assignment (1- 5) and arranged: a) LIDAR; b) GEOS-Chem
350 simulation; and c) GEOS-CF simulation.

351

352 The clustering analysis results provided a characterization of O₃ behavior that transpired during these three campaigns.

353 ~~Figure 3c indicates each cluster represents a different photochemical regime and is useful in that it could demonstrate~~

354 ~~background O₃ in the case studies. HLO curtain profiles also had higher background O₃, indicating these cases did not have~~

355 ~~“clean air” to begin with which have allowed for a greater accumulation in the low-level. Figure 3b and 3c indicate each cluster~~

356 ~~represents a different O₃ evolution pattern, likely related to different photochemical or transport regimes. This kind of~~

357 ~~evaluation is useful in that it combines O₃ information from both temporal and vertical dimensions. For example, the HLO~~

358 ~~cluster reveals the specific case in which higher O₃ is captured early in the temporal profile in the low-level and translates to~~

359 ~~the higher O₃ captured in the low-level as well. The profile curtains show higher background O₃, indicating these cases did not~~

360 ~~have “clean air” to begin with which can allow a greater accumulation in the low-level in the afternoon. This is an example of~~

361 ~~how this type of clustering analysis, if applied, could demonstrate background O₃ in the similar case studies.~~ In another

362 example, several profile curtains assigned to the HMO cluster indicate concentrated residual layers in the mid-level and

363 possible entrainment to the surface as the day progressed. To prove this feature, vertical velocity and vertical velocity variance

364 data would be needed but the knowledge that a clustering approach is able to pinpoint these features that could only be

365 discernible through lidar measurements proves to be useful. The clustering results was valuable in recognizing a significant

366 large pollution related cluster (HLO), a total of 18 out of the 91 curtain profiles which correspond with the highest daily surface

367 maxima measured at these sites (= 97.77 ppb) (Table 1). This cluster, on average, exhibited a daily surface maxima up to 10

368 ppb greater than any of the other clusters. Discerning these higher O₃ cases is imperative for mitigating severe air pollution.

369

370 **3.2. Cluster ~~meteorological~~ surface analysis**

371 To support the lidar clustering results, daily averaged meteorological surface observations from AQS stations pertaining

372 to the campaign period and GEOS-Chem surface model output were evaluated in regard to the five clusters. Figure 5 shows

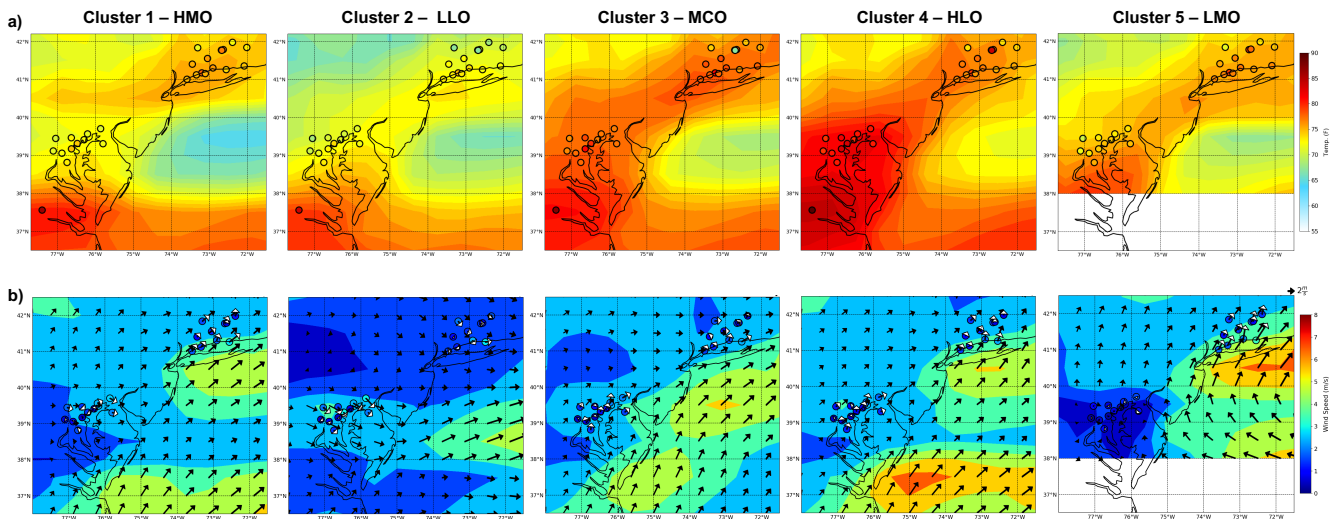
373 the cluster mean surface temperature from AQS stations and GEOS-Chem model as well as the simulated wind speed and

374 direction. The average surface temperature from each station is represented as the circular markers while the simulated

375 temperatures are represented as the spatial contour and the simulated wind speed (m s⁻¹) and direction as arrows. Cluster

376 average, minimum, and maximum AQS surface temperature and wind speed can be found in Table 1d, e.

377



378

379 **Figure 5.** Cluster averaged meteorological surface AQS station observations and GEOS-Chem model results. a) Surface
 380 temperature observations represented as the circular markers and simulated surface temperatures represented as the spatial
 381 contour (top-panel). b) Surface wind speed and direction observations represented as the circular markers and white arrows
 382 and simulated wind speed and direction represented as spatial contour and black arrows (bottom-panel).

383

384 In general, the surface meteorological conditions agree with our knowledge of transport and O_3 production that would
 385 lead to each of the five clustered lidar O_3 profile curtains. It is evident that the clusters with the highest surface O_3 (HMO,
 386 MCO, and HLO) all share a predominant offshore, westerly wind. Furthermore, MCO and HLO presented higher overall
 387 observed and simulated surface temperatures compared to the other clusters (Figure 5a). Observed and simulated wind speeds
 388 reveal slightly lower average wind speeds and primarily continental wind flow for both clusters as well (Figure 5b). These
 389 meteorological conditions are conducive to a higher production of surface O_3 concentrations which validates the higher O_3
 390 found in the low-level results (Figure 3b, 4a).

391 Conversely, the lowest surface temperatures are found in LLO. Lower surface temperatures are also indicative of low
 392 vertical mixing due to less generation of convection. Relatively calm wind speeds and lower temperatures indicate other
 393 possible meteorological factors such as high cloud cover that could have contributed to the lower O_3 concentrations in LLO.
 394 Although surface O_3 concentrations in LMO reach higher levels later in the day, first at 13:00 EDT and then again at 16:00
 395 EDT, the rest of the temporal profile stays below moderate levels. Average temperatures for LMO are moderately high but, in
 396 contrast, the average wind speed is higher (specifically over the Long Island Sound) and unique to the other clusters, wind
 397 direction is predominantly onshore (Easterly – Southerly). This prevalent onshore flow indicates a transport of cleaner marine
 398 air which corroborates the lower surface O_3 levels. LMO did not have any profile curtains assigned from OWLETS-1 which
 399 is why data for the lower Chesapeake Bay area is not shown in Figure 5.

400 There was only one occurrence during the dates in which the lidar instruments were operating in which there was a
401 recorded maximum daily 8-hour average (MDA8) O₃ exceedance (> 70 ppbv). This exceedance date is 25 May 2018 in which
402 3 AQS sites in the LISTOS region measured MDA8 O₃ of 73, 72, and 72 ppbv. This curtain profile was assigned to the HMO
403 cluster (Cluster 1), the cluster with high O₃ in the mid-level and moderate O₃ in the low-level and near the surface.

405 3.3. Evaluating the GEOS-Chem and GEOS-CF model

406 In this sect. the model results from GEOS-Chem and GEOS-CF will be compared to the lidar data using the five lidar O₃
407 profile clusters discussed in Sect. 3.1. Both model results were sampled in an equal manner, in which we extracted the same
408 cluster date assignments from the lidar clusters and created mean vertical profiles based on the model results. This allowed us
409 to evaluate the model performance based on the five characterized O₃ lidar clusters. As mentioned previously, the GEOS-CF
410 simulation data is not available for 2017. Thus, the results shown subsequently will only include GEOS-CF results from 2018
411 (only dates from the OWLETS-2 and LISTOS campaigns). The GEOS-Chem simulation results include both years thus all
412 three campaign duration periods.

414 3.3.1 Overall model performance

415 ~~In Figure 6, we first evaluate the overall relationship and correlation between both models and the lidar data, disregarding~~
416 ~~the specific clusters. The comparisons are separated by the two different altitude subsets as the performances are strikingly~~
417 ~~different between low level and mid level for both GEOS-Chem (Figure 6a) and GEOS-CF (Figure 6b). In general, the models~~
418 ~~perform better simulating O₃ behavior in the low level than the mid level for all five clusters.~~

419 ~~The overall correlation indicates that GEOS-CF ($R = 0.69$) has a slightly stronger correlation than GEOS-Chem ($R =$
420 0.66) in the low level (Figure 6 – top panel). For both models, correlation is higher than 0.51, signifying a fair relationship
421 between the model simulations and the lidar observations. The overall correlation reveals that GEOS-CF is marginally superior
422 to GEOS-Chem in the mid level but both models have a fairly weak relationship at this altitude range ($R = 0.22$ and $R = 0.12$,
423 respectively) (Figure 6 – bottom panel). The overall correlation analysis provides a fundamental but condensed assessment of
424 model performance. In the next sect., the cluster specific differences reveal additional model performance insight that would
425 be conceivably overlooked when evaluating overall performance.~~

426 ~~In evaluating the models based on the established O₃ behavior cases, significant cluster by cluster differences are~~
427 ~~unmasked. Figure 4b and 4c depict the simulated cluster mean O₃ profile curtains from GEOS-Chem and GEOS-CF, mirroring~~
428 ~~the mean lidar curtains in Figure 4a. For all clusters in the low level, both models simulate a continuous accumulation of O₃~~
429 ~~near the surface after 12:00 EDT, mirroring the O₃ common diurnal pattern depicted in mean lidar curtains in Figure 4a.~~
430 ~~However, the extent the models simulate is often higher in magnitude than the observations, specifically GEOS-CF predicting~~
431 ~~the accumulation at a higher magnitude than GEOS-Chem. In the mid level, both models simulate much less O₃ variability~~
432 ~~than what is captured in the lidar observations. Figure 4b and 4c clearly show how the models struggle to reproduce the intricate~~
433 ~~O₃ pattern and variability that is relayed in the lidar observations (Figure 4a), especially in the mid level. To compare and~~

434 quantify the results illustrated in Figure 4, modeled versus lidar observation spatial O_3 differences were derived for each cluster
435 (Figure 7). Figure 7 highlights the explicit spatiotemporal model differences compared to the lidar curtains for each cluster.
436 The cluster specific percent biases and correlation statistics, found in Table S1 and Figure S4 (in Supplementary Material),
437 were calculated from the total vertical and diurnal averages separated by low level and mid level.

438 ~~GEOS Chem performs well in simulating low level O_3 with a lower non systematic percent bias ranging from -0.051 to~~
439 ~~+0.068 % for the five clusters. GEOS Chem has a slightly lower correlation than GEOS CF in the low level ($R = 0.51 - 0.61$)~~
440 ~~but still indicates a reasonable relationship with the lidar observations. GEOS Chem also has a non systematic bias in the low~~
441 ~~level. Thus, GEOS Chem can simulate the variability of O_3 and based on the lower bias, the magnitude as well. In all five~~
442 ~~clusters, GEOS CF overestimates the average magnitude of low level O_3 with a systematic high positive percent bias ranging~~
443 ~~from +0.139 to +0.340 % (Table S1). GEOS CF has a relatively good correlation ($R = 0.54 - 0.74$) but a consistently high bias~~
444 ~~compared to the lidar observations (Table S1 and Figure S4, Supplementary Materials). From the estimated differences (Figure~~
445 ~~7), this can be attributed predominantly to GEOS CF overestimating afternoon O_3 .~~

446 ~~In the low level, GEOS Chem has the best performance (minimal +0.020 % bias) in LLO, which is the cluster with the~~
447 ~~lowest O_3 accumulation. The second best performance for GEOS Chem in the low level follows closely behind (minimal~~
448 ~~0.026 % bias) in HLO, the cluster with the highest O_3 accumulation. These results suggest GEOS Chem performs well in the~~
449 ~~low level but has a tendency to overpredict lower O_3 concentrations and underpredict higher O_3 concentrations. GEOS CF has~~
450 ~~a similar performance in the low level for HMO, LLO, and LMO with positive percent biases at 0.139, 0.189, and 0.197 %,~~
451 ~~respectively. This implies GEOS CF has a better ability capturing lower O_3 concentrations below 2000 m than higher~~
452 ~~concentrations, such as MCO and 4. Both models have the worst performance in MCO with a +0.068 % bias for GEOS Chem~~
453 ~~and +0.340 % bias for GEOS CF. As described in Sect. 3.1, MCO is the most common cluster with moderately high average~~
454 ~~O_3 concentrations (refer to Figure 3b). As both models have the highest bias for this cluster, this suggests neither model is fully~~
455 ~~able to simulate moderately high O_3 in the low level which was a frequently occurring event for this study period.~~

456 ~~In the mid level, GEOS Chem performs poorly, consistently underestimating O_3 to a significant magnitude. In all five~~
457 ~~clusters, GEOS Chem underestimates the magnitude of mid level O_3 with a systematic high negative percent bias ranging from~~
458 ~~-0.268 to -0.096 % (Table S1). GEOS Chem also has a low correlation in the mid level ($R = -0.26 - 0.23$). Thus, GEOS Chem~~
459 ~~is not able to simulate the variability of O_3 nor the magnitude well in the mid level. GEOS CF performs slightly better than~~
460 ~~GEOS Chem in simulating mid level O_3 with a lower and non systematic percent bias for the five clusters ranging from -0.143~~
461 ~~to +0.112%. GEOS CF has a marginally stronger correlation to the lidar observations than GEOS Chem for all clusters except~~
462 ~~MCO, where GEOS Chem has -0.26 correlation and GEOS CF has a -0.19 correlation (Figure S4, Supplementary Materials).~~
463 ~~Thus, GEOS CF, in some cases, is better able to simulate the O_3 variability in the mid level ($R = -0.19 - 0.74$) and based on~~
464 ~~the lower bias, the magnitude as well.~~

465 ~~Both models underestimate mid level O_3 magnitude to the greatest extent in HMO, which is the cluster with the highest~~
466 ~~mid level O_3 concentrations (refer to Figure 3c). This implies that the models struggle to simulate higher concentrations of O_3~~
467 ~~in the mid level (≥ 70 ppb). GEOS CF does best simulating LLO, MCO, and HLO, all clusters with moderate mid level O_3~~

468 averages (≤ 60 ppb). On the other hand, the GEOS-Chem model never reaches O_3 cluster averages greater than 50 ppb, which
469 directly divulges the greater systemic negative bias in the mid-level. GEOS-Chem simulates LMO mid-level O_3 the best ($-$
470 0.096 percent bias), which is the cluster with the lowest O_3 average (< 45 ppb) indicating GEOS-Chem is relatively capable of
471 simulating mid-level O_3 only when the case devises lower concentrations.

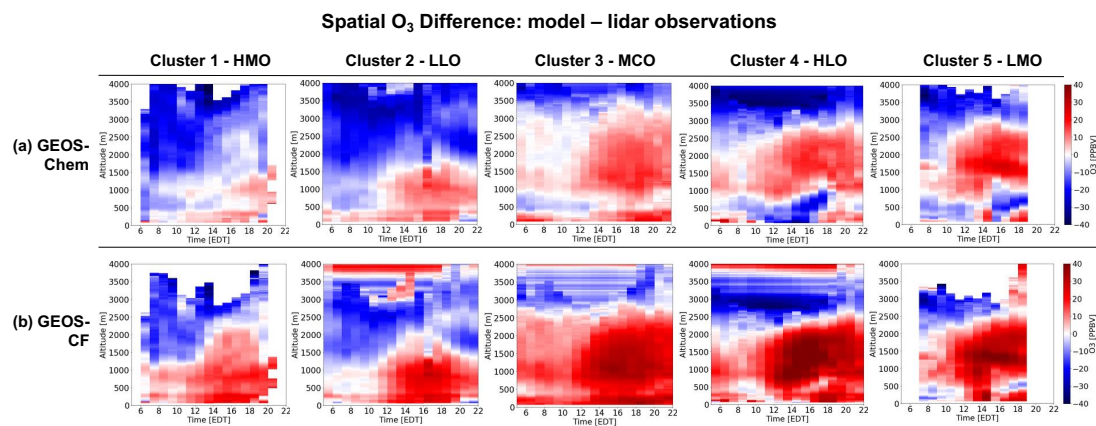
472 Figure 4b and 4c depict the simulated cluster-mean O_3 profile curtains from GEOS-Chem and GEOS-CF, mirroring the
473 mean lidar profile curtains in Figure 4a. For all clusters in the low-level, both models simulate a consistent accumulation of
474 O_3 near the surface after 12:00 EDT, mirroring the O_3 common diurnal pattern depicted in mean lidar profile curtains in Figure
475 4a. However, the extent the models simulate is often higher in magnitude than the observations, specifically GEOS-CF
476 consistently predicting the accumulation at a higher magnitude than GEOS-Chem. In the mid-level, both models simulate
477 much less O_3 variability than what is captured in the lidar observations. Figure 4b and 4c clearly show how the models struggle
478 to reproduce any mid-level O_3 pattern or variability that is relayed in the lidar observations. This is in contrast to the low-level
479 where the models are able to reproduce the common diurnal pattern of O_3 . With the lidar data providing a full temporal and
480 vertical profile curtain of O_3 behavior and development, we are able to indicate areas where the models struggle such as in this
481 case in the mid-level.

482 We first evaluate overall correlation and biases between the model and lidar data. The overall correlation between both
483 models and the lidar data, disregarding the specific clusters, based on the two altitude subsets as the performances differ
484 between low-level and mid-level for both GEOS-Chem (Figure S7a) and GEOS-CF (Figure S7b). The mean normalized biases
485 for the five clusters displayed in Table S1 (in Supplementary Material) were calculated from the total vertical and diurnal
486 averages separated by low-level and mid-level. For both models, overall low-level O_3 correlation rounds to 0.70, signifying a
487 strong relationship between the model simulations and the lidar observations (Figure S7 - top panel). This indicates that both
488 models can simulate the development and pattern of O_3 well in the low-level. Overall, GEOS-Chem performs well in
489 simulating low-level O_3 with a lower non-systematic normalized bias ranging from -0.10 to +0.13 for the five clusters. Thus,
490 based on the lower bias, GEOS-Chem fairs well simulating the magnitude of low-level O_3 as well. For all clusters, GEOS-CF
491 overestimates the average magnitude of low-level O_3 with a systematic high positive normalized bias ranging from +0.30 to
492 +0.67. This consistently high bias reveals that GEOS-CF generally is unable to simulate low-level O_3 magnitude well.

493 For the mid-level, the overall correlation reveals that GEOS-CF and GEOS-Chem both have a weak relationship with the
494 lidar ($R = 0.22$ and $R = 0.12$, respectively) (Figure S7 - bottom panel). This indicates that neither model is able to simulate
495 mid-level O_3 pattern well. GEOS-Chem consistently underestimates the magnitude of mid-level O_3 with a systematic high
496 negative normalized bias ranging from -0.44 to -0.18, for all clusters, while GEOS-CF has a lower and non-systematic
497 normalized bias ranging from -0.22 to 0.28. Overall, both models are not able to simulate the variability of O_3 nor the magnitude
498 well in the mid-level. The overall analysis in this sect. provides a fundamental but condensed assessment of model
499 performance. In the next sect., the cluster specific differences reveal additional model performance insight that would be
500 conceivably overlooked when evaluating overall performance.

501

502 3.3.2 Model evaluation based on lidar clusters

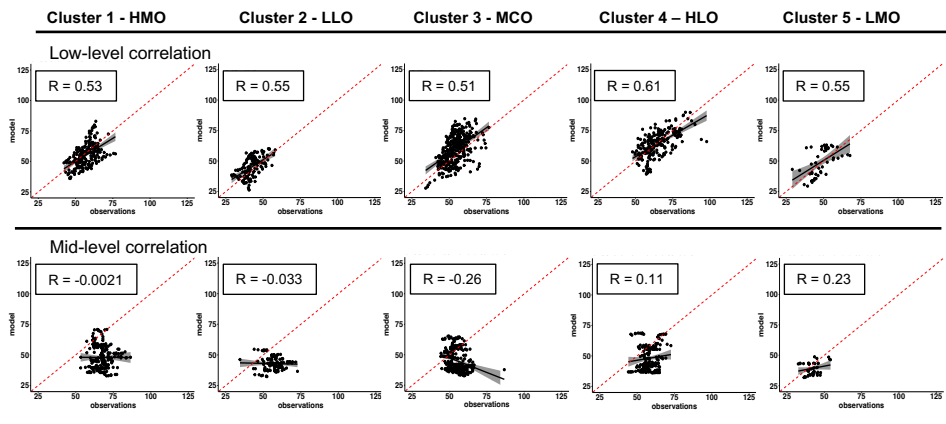


503

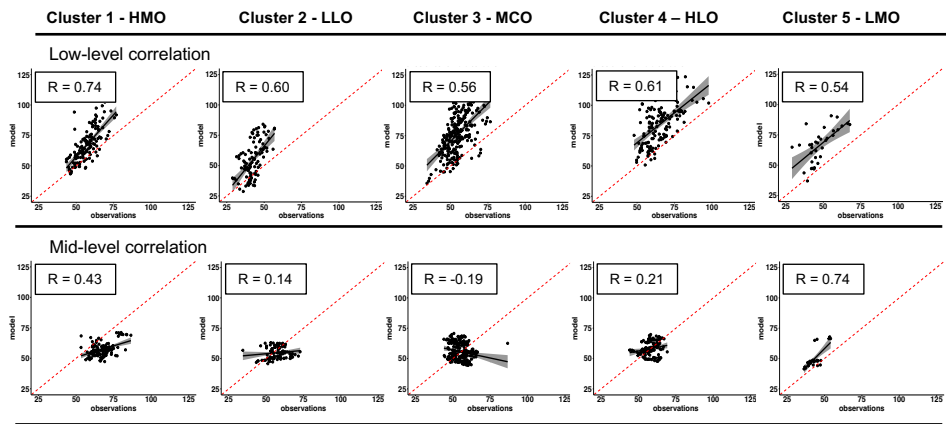
504 Figure 6. Mean profile curtain spatial O₃ difference (model – lidar observations) for each cluster (1 – 5). GEOS-Chem
505 differences (a) and GEOS-CF differences (b).

506

(a) GEOS – Chem model



(b) GEOS – CF model



507

508 **Figure 7.** O_3 correlation between lidar observations and a) GEOS-Chem model simulation results and b) GEOS-CF model
509 results by each cluster split by low-level (top panel) and mid-level (bottom panel).

510

511 ~~In evaluating the models based on the established O_3 behavior cases, significant cluster by cluster differences are~~
512 ~~unmasked. Figure 4b and 4c depict the simulated cluster mean O_3 profile curtains from GEOS-Chem and GEOS-CF, mirroring~~
513 ~~the mean lidar curtains in Figure 4a. For all clusters in the low-level, both models simulate a continuous accumulation of O_3~~
514 ~~near the surface after 12:00 EDT, mirroring the O_3 common diurnal pattern depicted in mean lidar curtains in Figure 4a.~~
515 ~~However, the extent the models simulate is often higher in magnitude than the observations, specifically GEOS-CF predicting~~
516 ~~the accumulation at a higher magnitude than GEOS-Chem. In the mid-level, both models simulate much less O_3 variability~~
517 ~~than what is captured in the lidar observations. Figure 4b and 4c clearly show how the models struggle to reproduce the intricate~~
518 ~~O_3 pattern and variability that is relayed in the lidar observations (Figure 4a), especially in the mid-level. To compare and~~
519 ~~quantify the results illustrated in Figure 4, modeled versus lidar observation spatial O_3 differences were derived for each cluster~~
520 ~~(Figure 7). Figure 7 highlights the explicit spatiotemporal model differences compared to the lidar curtains for each cluster.~~

521 ~~The cluster specific percent biases and correlation statistics, found in Table S1 and Figure S4 (in Supplementary Material),~~
522 ~~were calculated from the total vertical and diurnal averages separated by low level and mid level.~~

523 ~~—GEOS Chem performs well in simulating low level O₃ with a lower non-systematic percent bias ranging from -0.051~~
524 ~~to +0.068 % for the five clusters. GEOS Chem has a slightly lower correlation than GEOS CF in the low level (R = 0.51~~
525 ~~0.61) but still indicates a reasonable relationship with the lidar observations. GEOS Chem also has a non-systematic bias in~~
526 ~~the low level. Thus, GEOS Chem can simulate the variability of O₃ and based on the lower bias, the magnitude as well. In all~~
527 ~~five clusters, GEOS CF overestimates the average magnitude of low level O₃ with a systematic high positive percent bias~~
528 ~~ranging from +0.139 to +0.340 % (Table S1). GEOS CF has a relatively good correlation (R = 0.54 0.74) but a consistently~~
529 ~~high bias compared to the lidar observations (Table S1 and Figure S4, Supplementary Materials). From the estimated~~
530 ~~differences (Figure 7), this can be attributed predominantly to GEOS CF overestimating afternoon O₃.~~

531 ~~In the low level, GEOS Chem has the best performance (minimal +0.020 % bias) in LLO, which is the cluster with the~~
532 ~~lowest O₃ accumulation. The second best performance for GEOS Chem in the low level follows closely behind (minimal~~
533 ~~0.026 % bias) in HLO, the cluster with the highest O₃ accumulation. These results suggest GEOS Chem performs well in the~~
534 ~~low level but has a tendency to overpredict lower O₃ concentrations and underpredict higher O₃ concentrations. GEOS CF has~~
535 ~~a similar performance in the low level for HMO, LLO, and LMO with positive percent biases at 0.139, 0.189, and 0.197 %,~~
536 ~~respectively. This implies GEOS CF has a better ability capturing lower O₃ concentrations below 2000 m than higher~~
537 ~~concentrations, such as MCO and 4. Both models have the worst performance in MCO with a +0.068 % bias for GEOS Chem~~
538 ~~and +0.340 % bias for GEOS CF. As described in Sect. 3.1, MCO is the most common cluster with moderately high average~~
539 ~~O₃ concentrations (refer to Figure 3b). As both models have the highest bias for this cluster, this suggests neither model is fully~~
540 ~~able to simulate moderately high O₃ in the low level which was a frequently occurring event for this study period.~~

541 ~~In the mid level, GEOS Chem performs poorly, consistently underestimating O₃ to a significant magnitude. In all five~~
542 ~~clusters, GEOS Chem underestimates the magnitude of mid level O₃ with a systematic high negative percent bias ranging from~~
543 ~~-0.268 to -0.096 % (Table S1). GEOS Chem also has a low correlation in the mid level (R = -0.26 -0.23). Thus, GEOS Chem~~
544 ~~is not able to simulate the variability of O₃ nor the magnitude well in the mid level. GEOS CF performs slightly better than~~
545 ~~GEOS Chem in simulating mid level O₃ with a lower and non-systematic percent bias for the five clusters ranging from -0.143~~
546 ~~to +0.112 %. GEOS CF has a marginally stronger correlation to the lidar observations than GEOS Chem for all clusters except~~
547 ~~MCO, where GEOS Chem has -0.26 correlation and GEOS CF has a -0.19 correlation (Figure S4, Supplementary Materials).~~
548 ~~Thus, GEOS CF, in some cases, is better able to simulate the O₃ variability in the mid level (R = -0.19 -0.74) and based on~~
549 ~~the lower bias, the magnitude as well.~~

550 ~~Both models underestimate mid level O₃ magnitude to the greatest extent in HMO, which is the cluster with the highest mid-~~
551 ~~level O₃ concentrations (refer to Figure 3c). This implies that the models struggle to simulate higher concentrations of O₃ in~~
552 ~~the mid level (≥ 70 ppb). GEOS CF does best simulating LLO, MCO, and HLO, all clusters with moderate mid level O₃~~
553 ~~averages (≤ 60 ppb). On the other hand, the GEOS Chem model never reaches O₃ cluster averages greater than 50 ppb, which~~
554 ~~directly divulges the greater systemic negative bias in the mid level. GEOS Chem simulates LMO mid level O₃ the best (-~~

555 ~~0.096 percent bias), which is the cluster with the lowest O₃ average (< 45 ppb) indicating GEOS-Chem is relatively capable of~~
556 ~~simulating mid-level O₃ only when the case deviates lower concentrations.~~

557

558 Significant cluster by cluster differences are unmasked in evaluating the models based on the established O₃ behavior
559 cases. To quantify the results illustrated in Figure 4, we show spatial O₃ differences (model – lidar observations) for each
560 cluster (Figure 6) as well as individual cluster correlation (Figure 7) (subsequent cluster calculated normalized biases and
561 correlation can be found in Table S1). Evaluating the individual cluster biases and correlation reveal more in-depth model
562 discrepancies as well as areas where the models perform well.

563 In the low-level, GEOS-CF has a similar performance ability for the HMO, HLO, and LMO clusters with high positive
564 biases at + 0.30, + 0.41, and + 0.45 respectively. These higher biases imply GEOS-CF has difficulty capturing moderate O₃
565 concentrations below 2000 m (HMO and LMO) as well as the in the high O₃ cases (HLO). GEOS-CF also has a high positive
566 bias (+ 0.50) in the LLO cluster indicating that GEOS-CF struggles to capture the lower O₃ concentrations in the low-level.
567 This is warranted as models are intended to approximate and are not usually able to capture extremes (high or low) but GEOS-
568 CF also seems to struggle capturing moderate cases as well. In the low-level, GEOS-Chem has the best performance (minimal
569 -0.04 bias and strong correlation, R = 0.61) in HLO, which is the cluster with the highest low-level O₃ accumulation (refer to
570 Figure 4a). The second-best performance for GEOS-Chem in the low-level follows closely behind (minimal +0.07 bias and
571 fair correlation, R = 0.55) in LLO, the cluster with the lowest O₃ accumulation. These results suggest GEOS-Chem actually
572 performs well in cases of high O₃ as well as cases of low O₃ with a slight tendency to overpredict lower O₃ concentrations and
573 underpredict higher O₃ concentrations. This challenges the overall assumption that models struggle to capture extreme cases
574 since GEOS-Chem actually performs best in simulating both extreme cases of high O₃ in HLO and, again, low O₃ in LLO.
575 GEOS-Chem has a similar performance for the LMO and HMO clusters with negative biases of – 0.10 and – 0.09, respectively.
576 GEOS-Chem is also able to capture the moderate O₃ in both of these clusters well with slight underestimations.

577 Both models perform the worst (in comparison with the other clusters) in the low-level in the MCO cluster with a + 0.13
578 bias for GEOS-Chem and + 0.67 bias for GEOS-CF. As described in Sect. 3.1, MCO is the most common cluster with moderate
579 - high average O₃ concentrations in the low-level (refer to Figure 3b). Although GEOS-Chem has the worst performance in
580 the MCO cluster, it is not necessarily a poor performance. The performance follows the conclusion previously made that
581 GEOS-Chem can fairly simulate moderate O₃ in the low-level although, in this case, with slight overestimations. Contrarily,
582 the GEOS-CF performance in the MCO cluster reveals a more substantially high positive bias. This stands out as models are
583 usually able to capture moderate levels (e.g., non-extreme cases). Evaluating the full temporal and vertical profile indicates
584 that the higher GEOS-CF bias in the MCO cluster is additionally influenced by the greater overestimation of morning O₃, not
585 solely the afternoon O₃. This is different to the performance in the LLO and LMO clusters where GEOS-CF also had a high
586 positive bias in the low-level but does better simulating the early morning O₃ magnitude. A similar conclusion can be drawn
587 when evaluating the low-level GEOS-Chem performance. HMO, LLO, MCO, and LMO all share ‘higher’ biases (rounding to
588 +/- 0.10), but the highest bias is found in the MCO cluster. Analogous to GEOS-CF, this can similarly be attributed to GEOS-

589 Chem overestimating morning O₃ the worst in the MCO cluster in contrast to the better early morning estimation in the other
590 clusters.

591 In the mid-level, GEOS-Chem underestimates O₃ magnitude to the greatest extent in the HMO and the LLO cluster (both
592 bias = - 0.44), which are both clusters with higher mid-level O₃ concentrations (refer to Figure 3c). GEOS-Chem performs
593 similarly in the HLO and MCO clusters, with a negative mean bias of - 0.30 and - 0.27, respectively. This indicates that
594 GEOS-Chem most struggles to simulate higher concentrations of O₃ in the mid-level. The GEOS-Chem model actually never
595 reaches O₃ cluster averages greater than 50 ppb, directly divulging the greater systemic negative bias in the mid-level. GEOS-
596 Chem simulates LMO mid-level O₃ magnitude the best (- 0.18 bias), which is the cluster with the lowest O₃ average (< 45
597 ppb). Although for the LMO cluster GEOS-Chem has a lower bias, the correlation is still poor (R = 0.23) which indicates that
598 the model is relatively capable of simulating mid-level O₃ only when the case devises lower concentrations but still fails to
599 replicate any O₃ variability and pattern.

600 On the other hand, GEOS-CF does best simulating LLO, MCO, and HLO, which are all clusters with moderate O₃ in the
601 mid-level (≥ 50 and ≤ 70 ppb). GEOS-CF has the highest bias in the LMO cluster (+ 0.28), the cluster with the lowest mid-
602 level O₃ magnitude. GEOS-CF also has the strongest correlation in the same LMO cluster (R = 0.74). This is a unique case
603 where although GEOS-CF is not able to capture the magnitude in the mid-level, it is able to capture the pattern of low O₃ well.
604 Comparing the full multi-dimensional lidar and model mean profile curtains it is evident that in the LMO cluster, the GEOS-
605 CF model simulates a similar mid-level O₃ pattern in the early morning/afternoon that is captured in the mean lidar curtain
606 profile. The second worst performance for GEOS-CF is the underestimation of mid-level O₃ in the HMO cluster, contrarily
607 the cluster with the highest mid-level O₃ (≥ 70 ppb). This supports the previous conclusion that although GEOS-CF has a
608 relatively lower biases in the mid-level, the model still struggles to simulate the extreme O₃ cases. Although GEOS-CF
609 underestimates O₃ magnitude in the HMO cluster, it actually has a higher correlation than most of the other clusters (R = 0.43)
610 (Figure 7, Table S1). In comparing the full multi-dimensional lidar and model mean profile curtain (Figure 3), GEOS-CF does
611 a fair job connecting the mid-level higher O₃ pattern in the early morning that develops down to the low-level later in the
612 afternoon. From this we can draw a conclusion that GEOS-CF is better able to capture mid-level O₃ patterns earlier in the
613 temporal profile leading to higher correlations with the lidar.

614

615 **3.3.3 Cluster approach and model conclusions**

616 ~~Evaluating the clustered O₃ lidar profile curtains against CTMs allowed us to conclude that for cases of high O₃ in the~~
617 ~~low level, GEOS-Chem was able to simulate but underestimates the extent of high O₃ near the surface while GEOS-CF~~
618 ~~struggled to simulate and overestimates these high O₃ cases. Previous studies have found that excessive vertical mixing has~~
619 ~~led to overestimation of O₃ near the surface as well as underestimation of O₃ night-time depletion led to overestimation of O₃~~
620 ~~the next day (Dacie et al., 2020; Keller et al., 2021; Travis & Jacob, 2019). The titration that occurs at night after the initial~~
621 ~~afternoon build up requires successful simulation to prevent the model beginning the following day with higher O₃ than is~~
622 ~~observed which can lead to the overprediction of O₃ later that day. Therefore, in the given case there is an O₃ event that lasts~~

623 ~~more than one day (at the same lidar location), the model will likely underestimate O_3 night time depletion, overpredict~~
624 ~~morning O_3 , and subsequently overpredict the afternoon build-up. Being as there were multiple cases (17 total from HMO,~~
625 ~~MCO, and HLO) of multi-day high O_3 events, this is likely one of the main reasons for GEOS-CF overestimating afternoon~~
626 ~~O_3 in these high low level O_3 cases. In Figure 7, GEOS-CF exhibits the greatest midday O_3 overprediction in MCO and HLO.~~
627 ~~In HLO alone, there were 4 (out of 18) of the profiles that were consecutive while in MCO there were 8 (out of 28). This gives~~
628 ~~explanation for upwards of 22–29 % of the overestimation of O_3 in the profile curtains of these clusters. These multi-day O_3~~
629 ~~events are particularly important as they can indubitably lead GEOS-CF to higher overprediction of afternoon O_3 .~~

630 ~~Contrarily, GEOS-Chem underpredicts O_3 in the morning times which does not allow for the same build-up up of midday~~
631 ~~O_3 distinct in the lidar curtain profiles. This could explain why GEOS-Chem underpredicts the clusters with higher O_3~~
632 ~~concentrations in the low level. Additionally, the low and non-systemic bias in the low level for GEOS-Chem demonstrates~~
633 ~~that the model does not have such an issue simulating the correct magnitude of O_3 but instead, the lower correlations suggest~~
634 ~~that GEOS-Chem merely struggles to simulate the pattern. This is most apparent in the MCO cluster where GEOS-Chem~~
635 ~~predicts a spatially larger build-up of O_3 but essentially does well in simulating the correct magnitude. This model gap can~~
636 ~~then be attributed to the coarser model resolution not being able to reproduce finer O_3 pattern behavior such as is evident in~~
637 ~~the lidar curtain profiles.~~

638 ~~In the mid-level GEOS-Chem has a systemic high negative bias for all clusters except the LMO cluster. It is evident that~~
639 ~~the model cannot simulate cases with higher O_3 concentrations in the mid-level. On the other hand, GEOS-CF performs better~~
640 ~~with a lower non-systemic bias in the mid-level. Since GEOS-Chem was run with the trophem chemistry mechanism which~~
641 ~~excludes stratospheric chemistry and GEOS-CF uses the UCX chemistry mechanism that includes stratospheric chemistry,~~
642 ~~this may allude to better performance of GEOS-CF in simulating higher O_3 concentrations in the mid-level. Both models~~
643 ~~indicate weak correlations with the lidar observations in the mid-level and it is apparent that both models struggle to capture~~
644 ~~the pattern of O_3 behavior in the mid-level. This is likely due to the model resolutions. Although GEOS-CF has a finer~~
645 ~~resolution than GEOS-Chem, it still may not be sufficient in horizontal and vertical grid resolution to replicate the finer O_3~~
646 ~~variations captured in the 2-D lidar observations.~~

647 ~~Although this analysis proves to be a useful technique to characterize O_3 behavior over a period of time and to evaluate~~
648 ~~the ability of model to simulate the largely variable O_3 behavior, there are also limitations. In this study we are comparing~~
649 ~~single point lidar versus model output, therefore we cannot simply state that the model is incorrect. We make conclusions and~~
650 ~~draw biases based on the ability to subset a grid point and compare that to a single point lidar curtain to the best ability but~~
651 ~~there is still uncertainty. Ozone lidars have a unique advantage, compared to traditional surface measurements, in measuring~~
652 ~~vertical distribution of O_3 with respect to time. The high vertical and spatiotemporal resolution reveal intricate details about~~
653 ~~the behavior of O_3 during these campaigns. Lidars still have limitations that prove to be a complication e.g., noise signal and~~
654 ~~manual operations. At the time of writing, the operative limitation has been addressed and the lidars are now more fully~~
655 ~~automatized which removes some of the difficulty.~~

656 ~~Several studies rely on case study investigations to evaluate model performance in coastal regions. Another approach,~~
657 ~~demonstrated in Sect. 3.3.1, would be to simply group data by altitude to achieve a summarized model evaluation. However,~~
658 ~~a systematic and comprehensive understanding of the different photochemical regimes in coastal regions does not only require~~
659 ~~case studies and overall summaries. The clustering approach allows for a comprehensive yet still detailed evaluation of the~~
660 ~~different photochemical regimes in coastal regions and the model performances in these cases. Looking at the overall~~
661 ~~correlations (Figure 6), both models seem to have a good relationship with the low-level lidar observations. But, in applying a~~
662 ~~clustering method we can analyze cluster-by-cluster differences (Figure 7) and the gaps within the models are elucidated.~~
663 ~~Using the clustering, we are able evaluate how the cluster specific differences reveal additional model performance insight~~
664 ~~that would be conceivably overlooked when evaluating overall performance.~~

665
666 Several studies rely on case study investigations or grouping data by altitude to evaluate model performance. As
667 demonstrated in Sect. 3.3.1, we can evaluate the overall summarized the model profile curtains O₃ against the lidar profile
668 curtains and come to the simple conclusion that both models fairly simulate low-level O₃ but struggle to simulate mid-level
669 O₃. However, a systematic and comprehensive understanding of the different photochemical regimes in coastal regions does
670 not only require case studies and overall summaries. The clustering approach allows for a comprehensive yet still detailed
671 evaluation of the different photochemical regimes in coastal regions utilizing the lidar derived full profile curtains.
672 Additionally, using the clusters, we can efficiently evaluate the ability of the models to simulate many different cases of O₃.
673 This approach revealed specific O₃ cases in which the models perform well and others where the models fail that would have
674 been overlooked by solely considering the overall results. Using the clustering, we are able evaluate how the cluster specific
675 differences (Figure 6, Figure 7 and Table S1) reveal additional model performance insight and specific gaps that would be
676 conceivably overlooked when evaluating overall performance.

677 It is warranted that models struggle simulating extreme events/cases such as seen in the low-level in the HLO cluster and
678 in the LLO cluster. However, GEOS-Chem performs best in both clusters with minimal biases and strong to fair correlations.
679 Our result suggest that GEOS-Chem does a much better job simulating extreme O₃ cases in the low-level than expected. This
680 specific model feature is not eminent when evaluating overall performance. Additionally, overall GEOS-Chem performs
681 poorly in the mid-level. The detailed analysis granted by the cluster approach reveals GEOS-Chem has the lowest bias in the
682 LMO cluster signifying the model is better able to capture low O₃ conditions in the mid-level. The overall high systemic
683 positive bias for GEOS-CF in the low-level is further dissected when evaluating the individual clusters. GEOS-CF
684 systematically overestimates low-level O₃, but the individual clusters indicate that the model has a better correlation with O₃
685 in HMO cases. An even more profound case is exposed in which GEOS-CF has a strong correlation with mid-level O₃ in the
686 LMO cases despite having a low correlation overall. This concludes that in cases where the GEOS-CF model struggles to
687 reproduce O₃ concentrations, the model can still capture the O₃ variability seen by the lidar measurements.

688 The clustering approach also reveals more discrepancies in the models such as in the MCO cluster. The advantage of
689 evaluating full temporal and vertical profile curtains indicates that overestimation of early morning O₃ throughout the low-

690 level leads to the poorer performances in MCO for both models. The overestimation of morning O₃ in GEOS-CF adds to the
691 systemic overestimation in afternoon O₃ contributing the greater bias and poorer correlation. The same case can be found in
692 the GEOS-Chem MCO cluster performance but to a lesser extent as GEOS-Chem has a much lower positive bias. Previous
693 studies have found that excessive vertical mixing leads to overestimation of O₃ near the surface as well as underestimation of
694 O₃ night-time depletion resulting in overestimation of O₃ the next day (Dacic et al., 2020; Keller et al., 2021; Travis &
695 Jacob, 2019). The titration that occurs at night after the initial afternoon build up requires successful simulation to prevent the
696 model beginning the following day with higher O₃ than is observed which can lead to the overprediction of O₃ later that day.
697 Therefore, in the given case where there is an O₃ event that lasts more than one day (at the same lidar location), the model will
698 likely underestimate O₃ night-time depletion, overpredict morning O₃, and subsequently overpredict the afternoon build-up.
699 Given multiple cases of multi-day high O₃ events from the lidar measurements (17 total from HMO, MCO, and HLO), this is
700 likely one of the reasons for GEOS-CF overestimating early and therefore afternoon O₃ in these high O₃ cases in the low-level.
701 In Figure 6, GEOS-CF exhibits the greatest afternoon O₃ overprediction in MCO and HLO. In HLO alone, there were 4 (out
702 of 18) of the profiles that were consecutive while in MCO there were 8 (out of 28). This gives explanation for upwards of 22
703 – 29 % of the overestimation of O₃ in the profile curtains of these clusters. These multi-day O₃ events are particularly important
704 as they can indubitably lead the models to higher overprediction of afternoon O₃. As the full lidar profile curtains reveal, the
705 models tend to overestimate early morning O₃ in the MCO cases which links to the overestimation in afternoon O₃ as well.

706 Both models have a better ability to simulate early morning O₃ magnitude and pattern for other clusters than the MCO.
707 For example, GEOS-CF does best simulating morning low-level O₃ in cases of lower O₃ extent (LLO and LMO). Excluding
708 MCO, GEOS-Chem does not have such an issue overestimating low-level O₃ in the afternoon. In the other clusters, GEOS-
709 Chem actually underpredicts early morning low-level O₃ in the full vertical profile. An underestimation of early morning O₃
710 does not warrant the same build-up up of afternoon O₃. This gives some explanation to why GEOS-Chem underpredicts the
711 other clusters with higher O₃ concentrations in the low-level (HMO and HLO). In the mid-level GEOS-Chem has a systemic
712 high negative bias for all clusters, consistently underestimating O₃ but the clusters reveal a better performance in LMO, the
713 cluster with lowest mid-level O₃ extent. It is evident that the model cannot simulate cases with higher O₃ concentrations in the
714 mid-level but simulates low O₃ cases better. On the other hand, GEOS-CF results indicate a lower non-systemic bias in the
715 mid-level. Since the version of GEOS-Chem used in this study was run with the tropchem chemistry mechanism which
716 excludes stratospheric chemistry (now obsolete with current GEOS-Chem developments) and GEOS-CF uses the UCX
717 chemistry mechanism that includes stratospheric chemistry, this may allude to better performance of GEOS-CF in simulating
718 higher O₃ concentrations in the mid-level. Both models indicate weak correlations with the lidar observations in the mid-level
719 and it is apparent that both models struggle to capture the pattern of O₃ behavior in the mid-level. This could be due to multiple
720 model inefficiencies such as the coarse model resolutions. Although GEOS-CF has a finer resolution than GEOS-Chem, it still
721 may not be sufficient in horizontal and vertical grid resolution to replicate the O₃ variations captured in the 2-D lidar
722 observations.

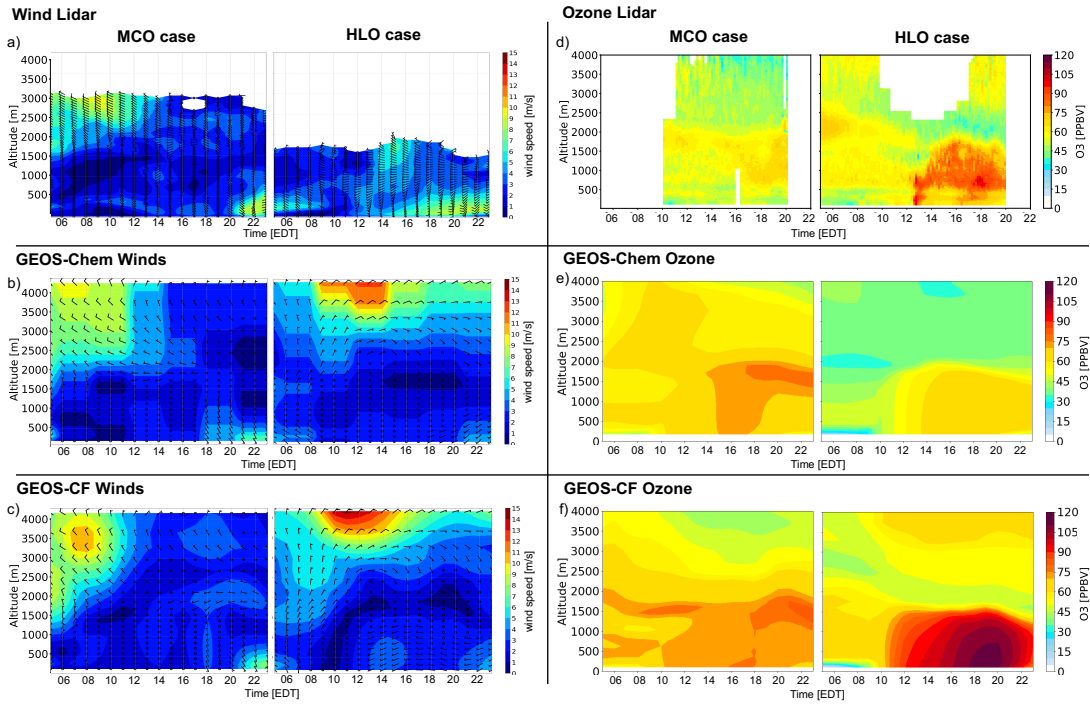
723 There are additional model discrepancies that can lead to underestimations of O₃ in GEOS-Chem in the mid-level that
724 was found in all 5 clusters. One gap in the GEOS-Chem model could be the representation of tropospheric halogen chemistry
725 which has a large effect of coastal O₃ production. Newer updates to the GEOS-Chem model (v12.9) have included updated
726 tropospheric halogen chemistry mechanisms (iodine, bromine, and chlorine) (Wang et al., 2021). This study found that the
727 updated halogen chemistry actually worsens the overall underestimation of O₃ throughout the troposphere, specifically in the
728 northern hemisphere, indicating further investigation of halogen chemistry is needed for better model representation. Another
729 study finds a similar conclusion in the proper representation of cloud uptake and tropospheric chemistry (Holmes et al., 2019).
730 This study found that implementing an updated, more accurate, and stable cloud entrainment-limited uptake in the GEOS-
731 Chem model reduces the sensitivity of oxidants and aerosol chemistry in the troposphere but still had little effect on O₃ model
732 comparison to observations (such as sonde and aircraft). This is due to the environmental variability being much higher than
733 the effect of NO_x and O₃ cloud chemistry but still warrants further testing. The role lightning plays in tropospheric oxidation
734 is another feature that is commonly misrepresented in global models and can affect O₃ simulation (Mao et al., 2021). These
735 are all examples of features that if not simulated correctly can lead to misestimations of O₃. The clustering approach allows us
736 to organize the detailed lidar measurements to scope out specific cases where these misrepresentations occur. These previous
737 studies also highlight the importance of lidar measurements and their ability to depict tropospheric emission development and
738 behavior throughout the vertical profile and diurnal cycle which can be used to constrain model emissions and improve
739 simulations.

740 Although this analysis proves to be a useful technique to characterize the largely variably O₃ behavior in coastal regions
741 and evaluate the subsequent model performance, there are also limitations. In this study we are comparing single point lidar
742 versus model output, therefore we cannot simply state that the model is incorrect. We make conclusions and draw biases based
743 on the ability to subset a grid point and compare that to a single point lidar curtain to the best ability but that still leaves an
744 uncertainty. The high vertical and spatiotemporal resolution reveal intricate details about the behavior of O₃ during these
745 campaigns. O₃ lidars have a unique advantage, compared to traditional surface measurements, in measuring vertical
746 distribution of O₃ with respect to time. This advantage is of great value when investigating model ability in simulating the
747 spatial and temporal distribution of O₃ and can provide crucial information in understanding surface O₃ events.

749 ~~3.4 Impact of meteorological factors on clusters & model performance~~ Cluster derived case studies to evaluate modeled 750 wind and ozone

751 Meteorological factors such as wind speed and direction can directly impact whether a coastal region will experience
752 clean air or O₃ exceedances. When local meteorological processes such as sea/bay breeze occur at such a fine scale, equally
753 fine resolution measurements are essential in capturing this. The Doppler wind lidar offers a focus on fine details that are only
754 revealed in the multi-dimensional data which allows for such a comprehensive evaluation of the established O₃ cluster profile
755 curtains. In this sect., we evaluate the 2-D relationship between wind and O₃ to assess model performance using lidar and
756 model derived profile curtains (Figure 8). We derived two specific case studies, each from a different cluster: MCO = 17 June

757 2018 and HLO = 30 June 2018. Utilizing the derived clusters, the case studies were chosen to focus on high low-level O₃
 758 behavior cases with a goal of evaluating possible sea/bay breeze events. The two case studies are both from the HMI location
 759 during the OWLETS-2 campaign. There are consistent Doppler lidar measurements throughout the low-level (<2000 m) which
 760 allows for a direct comparison with the simulated profiles; therefore, the focus of the following analysis will be on the low-
 761 level altitudes. The deficit of mid-level observed wind data disallows for a conclusive and concrete evaluation of simulated
 762 mid-level O₃.



763
 764 **Figure 8.** Profile curtains of wind speed/direction (a-c) and ozone (d-f) from the lidar (top panel), GEOS-Chem (middle panel),
 765 and GEOS-CF (bottom panel). Results from OWLETS-2 at HMI.

766
 767 **3.4.1 Doppler wind lidar and simulated wind case studies Sea breeze event interpretation**

768 GEOS-Chem and GEOS-CF both struggle to capture low-level wind speed and direction in both MCO and HLO cases
 769 (Figure 8a-c). In the MCO case, the Doppler wind lidar captures a wind direction shift from westerly to easterly winds
 770 beginning at 06:00 EDT accompanied by calm winds (approximately 0 m s⁻¹) indicating a likely common sea/bay breeze event.
 771 The timing of the start of this event is simulated well but the models fail to predict an actual well-defined wind shift, instead
 772 merely simulating 0 m s⁻¹ winds after 05:00 EDT. It is apparent that the models struggle to capture the finer processes such as
 773 a sea/bay breeze which could have likely led the underprediction of wind speed. It is important to note that GEOS-Chem runs
 774 with offline meteorology, averaged every 3 hours. Since sea/bay breezes often happen at a finer temporal resolution, the GEOS-
 775 Chem model is at a disadvantage in modelling such fine processes. A wind direction shift is also depicted in the HLO case,

776 with westerly winds early in the morning and a shift to south-easterly winds later in the temporal profile (at about 10:00 EDT).
777 This could also likely be an early onset sea breeze event which could have contributed to the high observed O₃ concentrations
778 in the afternoon. Again, the exact timing of the start of the wind shift is captured by the models but then no defined directional
779 shift and little to no winds are simulated after. Both the MCO case and HLO case observe increased wind speeds near the
780 surface, first before 08:00 EDT then again in the evening. Both models underestimate the extent of the increased wind speeds.

781

782 3.4.2 Ozone and winds in relation to lidar measurements-Relation to ozone cases and clustering

783 In this sect., the wind lidar curtains will be assessed in relation to the O₃ lidar profile curtains and the model performance.
784 The results in sect. 3 revealed that both models had the highest bias and lowest correlation simulating low-level O₃ in MCO.
785 Evaluating the wind and O₃ lidar profile curtains against the model simulations helps paint a better picture as to why. Similar
786 to the MCO cluster mean curtain profile, early morning low-level O₃ in each case is overestimated by both models (Figure 8e,
787 f). There is higher O₃ captured in the lidar curtain profile, but it is constrained between 1500 – 2000 m. Both models bring this
788 higher O₃ pattern down to the surface (below 500 m) overestimating O₃ throughout the low-level. Since both models predict
789 little to no winds during this time, this could contribute to overestimations of O₃ near the surface.

790 In the HLO case, GEOS-CF overestimates low-level O₃ while GEOS-Chem underestimates low-level O₃. From sect. 3.3
791 the results revealed that although GEOS-CF has a high positive normalized bias for low-level O₃ in HLO, the model had a
792 reasonable relationship (R = 0.61) with the O₃ lidar measurements. This is corroborated with the individual HLO case (Figure
793 8f) as GEOS-CF is better able to simulate the development of O₃ in the low-level, especially in the early morning. The GEOS-
794 CF modeled winds mirror this performance with a better reproduction of the wind shift in HLO (Figure 8c). While GEOS-
795 Chem has a lower normalized bias for low-level O₃ in the HLO cluster, GEOS-Chem consistently underestimates wind speed
796 and fails to reproduce any wind shifts. This reveals that in the possible sea breeze event, the two models do not perform equally.
797 Since GEOS-Chem is an offline CTM using archived meteorology and GEOS-CF simulates atmospheric composition
798 simultaneously with meteorology (online), the replication of a sea breeze case would not necessarily be comparable.

799 In most cases, sea/bay breeze events can contribute to high concentrated daytime O₃ events in which O₃ is recirculated
800 throughout the region. Such cases would likely lead to a similar curtain profile as seen in the HLO case (Figure 8a), where
801 high O₃ in the morning is likely associated with the higher O₃ at the surface in the afternoon. But it is apparent that the cases
802 for MCO and HLO are dissimilar. We would expect per the clustering approach that sea breeze cases would most likely be
803 assigned to the same cluster, but this is not the case here. Investigating the full lidar and model profile curtains for the two
804 cases gives us more information as to why these two curtains are not in the same cluster. It is evident that the HLO case has
805 much higher afternoon O₃ near the surface (below 1000 m) than the MCO case, with peaks > 75 ppb at both 12:00 and again
806 at 16:00 EDT. In contrast, the MCO case has higher afternoon O₃ concentrations captured above 2000 m than the HLO case.
807 The HLO case has high O₃ in the afternoon, but it is constrained to the lower 2000 m and just above this high O₃ plume, there
808 is an O₃ deficit of almost 50 ppb. Although the MCO case also reveals lower O₃ above 2000 m, the vertical gradient in this
809 case is not as stark. This is also replicated in both models which simulate lower O₃ directly above the high surface O₃ in the

810 HLO cluster but simulate much higher O₃ above 2000 m in the MCO cluster. From their distinct vertical and temporal behavior,
811 it is easy to conclude why these two cases were not assigned to the same cluster.

812 The cases elected for MCO and HLO give reason to address the difficulty simulating complex coastal mechanisms.
813 Despite the fact that MCO and HLO both indicated prospective sea/bay breeze cases, the results of the simulated winds and
814 O₃ were distinctive. Simulating complex sea/bay and land relations is imperative for correctly mitigating high O₃ cases. To
815 accurately simulate such complex exchanges, high resolution vertical and horizontal simulations are needed. Because of the
816 models' relatively coarse resolutions (nominally 50 and 25 km horizontal resolution; 72 vertical levels), the fine-scale vertical
817 wind gradients and horizontal wind shifts are difficult to resolve and, in these cases, not fully able to replicate. This study also
818 acknowledges the need for an evaluation of other modeled factors, such as divulged in sect. 3.3.3, considering the possible
819 confounding effects on modeled O₃ outcome.

820

821 **4. Conclusion**

822 We developed and tested a clustering method on a suite of 91 multi-dimensional lidar O₃ profile curtains retrieved
823 from three recent land/sea campaigns (OWLETS-1, OWLETS-2, and LISTOS), during the summer months of 2017 and 2018.
824 The K-Means clustering algorithm, driven by 8 well defined features, was applied to categorize the fine resolution O₃ data,
825 revealing five distinct O₃ behavior cases that are ~~unique~~ distinct in pattern and magnitude vertically and temporally. We present
826 five different clusters of O₃ behavior identified as: highest mid-level O₃ (HMO) cluster; lowest low-level O₃ (LLO) cluster;
827 most common O₃ (MCO) cluster; highest low-level O₃ (HLO); lowest mid-level O₃ (LMO) cluster. The results indicate that
828 fine resolution data can be used to differentiate the behavior of O₃ in a region and classify different cases of O₃ exploiting the
829 multiple dimensions. The clustering approach allowed us to characterize the range of highly variable vertical and temporal
830 coastal O₃ behavior for the duration of these campaigns which can be a good indicator of how O₃ behaves in general in these
831 coastal regions during the summer months. Furthermore, this approach could be used by states to better identify different O₃
832 photochemical regimes and frequency beyond just surface sampling.

833 ~~The clustering analysis provided an abridged method to~~ We evaluated the performance of two CTMs, GEOS-Chem
834 and GEOS-CF, in these complex environments. Overall, the models have the greatest difficulty simulating the vertical extent
835 and variability of O₃ concentrations in the mid-level, with ~~weak~~ overall relationships to the lidar observations (R = 0.12 and
836 0.22). GEOS-Chem had a systematic high negative bias and GEOS-CF an overall lower unsystematic bias range. In the low-
837 level, GEOS-Chem had overall low unsystematic bias range and fair relationship with the lidar observations (R = 0.66), while
838 GEOS-CF had a systematic high positive bias but overall fair relationship (R = 0.69).

839 Utilizing the curated clusters reveals new model insight that is neglected in the overall performance analysis. The
840 cluster approach divulges specific model limitations but also cases in which the models perform well. GEOS-Chem simulates
841 low-level O₃ cases best in the HLO and LLO clusters and the worst in the MCO cluster. HLO and LLO are the clusters with
842 the most extreme (low and high) O₃ cases while MCO is the most common cluster with moderate O₃. This concludes that
843 GEOS-Chem does best simulating extreme low-level O₃ but struggles to capture the frequently occurring moderate O₃

844 behavior. GEOS-CF also has the greatest overestimations for low-level O₃ in the MCO cluster. Evaluating the full profile
845 curtain reveals that this overestimation can be most attributed to the greater overestimation of early morning O₃. This feature
846 is unique to the MCO cluster and warrants further investigation as O₃ left in the residual layer can contribute to higher O₃ in
847 the afternoon and proves to be a challenge for CTMs. The value of lidar measurements is reflected in its ability to reveal these
848 features.

849 Both models share poor performances in the mid-level but there are specific cases that stand out in the clustering
850 results, specifically the LMO cluster, in which GEOS-CF shares a good agreement with the lidar measurements. It can be
851 concluded that although the model struggles to simulate O₃ magnitude, it can relatively emulate the mid-level O₃ pattern in
852 LMO. This is also apparent in the MCO cluster, in which the pattern of higher mid-level O₃ that suggests a relationship with
853 the low-level O₃ is simulated fairly in the GEOS-CF model. This pattern is also a rare feature that is captured in the lidar that
854 demonstrates the significance of the measurements. The greater underestimations of mid-level O₃ for GEOS-Chem can be
855 alluded to multiple model discrepancies. Since the GEOS-Chem version and mechanism used in this study (tropchem) only
856 considers tropospheric chemistry we can expect the performance in the mid-level to have deficiencies. Although GEOS-CF is
857 run with the combined tropospheric and stratospheric chemistry mechanism, has a better grid resolution, and is an online
858 model, there are still limitations to both models especially when simulating mid-level O₃. Known model errors and coarse
859 horizontal and vertical grid resolution contribute to the difficulty in simulating fine-scale coastal O₃ variability. There are many
860 contributing model factors that can be affecting the performance of GEOS-Chem and GEOS-CF that were mentioned in this
861 study not solely coarse model resolution.

862 A unique value of the clustering approach on multi-dimensional lidar data is that it offers a convenient way to ascertain
863 different O₃ case studies. An example of this is our evaluation of two cases studies from the MCO and HLO clusters. Modeled
864 winds were evaluated using Doppler wind lidar data observed during the OWLETS-2 campaign. The wind lidar data was
865 mostly limited to lower altitudes (< 2000 m), which allowed for wind speed and direction validation at the low-level. The
866 morning wind deceleration and directional shifts (onshore to offshore) illustrated in lidar profile curtains indicate a possible
867 sea/bay breeze event in both case studies. This is likely another contributor that led to enhanced surface O₃ in these cases. Due
868 to the coarser model resolution, GEOS-Chem and GEOS-CF were not able to capture the sea breeze phenomena in these cases
869 which could have facilitated in the high O₃ biases for these clusters. With GEOS-CF having a finer horizontal resolution than
870 GEOS-Chem, the results reveal minimal advantages ~~for GEOS-CF~~ simulating the pattern of wind speeds better but none the
871 ~~finer resolution did not help~~ in simulating the wind directional shifts ~~as in MCO and HLO~~. This affirms that the spatial
872 resolution of GEOS-CF (~25 km) is still not fine enough for mesoscale processes such as the sea/bay breeze. Although a
873 regional model analysis is out of the scope of this study, we propose to use multi-dimensional lidar measurements to evaluate
874 finer regional modeling in our future work. We acknowledge that other factors, aside from model resolution, contribute to
875 discrepancies in modeled coastal O₃ and further warrant a deeper evaluation. The clustering approach on lidar measurements
876 offers an unmatched ability to pinpoint these features.

877 ~~Ultimately, the vertical resolution for both models was too coarse to resolve fine-scale vertical wind gradients. We~~
878 ~~acknowledge that an evaluation of other factors, such as model precursor emissions or chemical mechanisms, is needed to~~
879 ~~fully evaluate the discrepancies in modeled coastal O₃.~~

880 This work is the first time that all three associated campaign lidar data have been analyzed in conjunction. In utilizing
881 the highly detailed suite of multi-dimensional lidar data, we are able to comprehensively explore the behavior and variability
882 of coastal O₃ for the duration of the campaigns. Applying the clustering analysis directly to the lidar O₃ data emerges as a
883 useful and robust approach for identifying O₃ patterns during the highly polluted summer months in coastal environments.
884 Since the time of the OWLETS and LISTOS campaigns, the lidar instrument systems have been updated and are now more
885 fully automatized for use eliminating such constraints faced in this study. Further observations using lidar instruments should
886 be especially valuable in investigating coastal O₃ behavior as it can divulge the finer-scale O₃ characteristics that remain
887 difficult to successfully simulate in CTMs. The time-height and fine resolution measurements only available from multi-
888 dimensional lidar instruments were vital in allowing us to form these conclusions.

889 This kind of evaluation allows for detailed model assessment of specific O₃ cases that are unmasked through the
890 clustering analysis. Looking at the overall correlations, it would seem the models have a good relationship with the low-level
891 lidar observations but looking into the cluster-by-cluster differences, the gaps within the models are elucidated. Using the
892 cluster assignments, we are able evaluate how the cluster specific differences reveal additional model performance insight that
893 could be conceivably overlooked when evaluating overall performance. This work is a middle ground between looking at
894 specific cases (or dates) and summarizing overall model performance. Additionally, the clustering approach provides an
895 abridged way to detecting distinctive case studies. We provide a new approach that allows a synopsis of summer coastal O₃
896 behavior and subsequently model performance without completely muting distinct O₃ features. Evaluating model performance
897 for diverse O₃ behavior in coastal regions is crucial for improving the simulation and furthermore, mitigation of air quality
898 events.

899 *Code availability.* Model code is available upon request to the first author.

900 *Data availability.* The GEOS-Chem model simulation data from this study is publicly accessible online at
901 <https://doi.org/10.7910/DVN/V99LHT>. The GEOS-CF model data is publicly available online at their website
902 https://gmao.gsfc.nasa.gov/-weather_prediction/GEOS-CF/. The lidar data is publicly available online at [https://www-](https://www-air.larc.nasa.gov/missions.htm)
903 [air.larc.nasa.gov/missions.htm](https://www-air.larc.nasa.gov/missions.htm).

904 *Supplement.*

905 *Author contributions.* CB and YW conceived the research idea. CB wrote the initial draft of the paper and performed the
906 analyses and model development. All authors contributed to the interpretation of the results and the preparation of the paper.

907 *Competing interests.* The authors declare that they have no conflict of interest.

908 *Acknowledgements.* This study is supported by NASA MUREP Graduate Fellowship (80NSSC19K1680). The Ozone Water-
909 Land Environmental Transition Study (OWLETS-1, 2) and Long Island Sound Tropospheric Ozone Study (LISTOS) field
910 measurements described here were funded by the NASA's Tropospheric Composition Program and Science Innovation Fund
911 (SIF), Maryland Department of Environment, the National Oceanic and Atmospheric Administration (NOAA), the
912 Environmental Protection Agency (EPA), the Northeast States for Coordinated Air Use Management (NESCAUM), and the
913 New Jersey and Connecticut Departments of Energy and Environmental Protection. The authors acknowledge the principal
914 investigators and data operators John Sullivan, Joel Dreessen, Ruben Delgado, William Carrion, and Joseph Sparrow as well
915 as the guidance of the Tropospheric Ozone Lidar Network (TOLNet). LMOL and TROPOZ data are publicly available at
916 (<https://www-air.larc.nasa.gov/missions/TOLNet/>). The OWLETS and LISTOS data are available at ([https://www-](https://www-air.larc.nasa.gov/)
917 [air.larc.nasa.gov/](https://www-air.larc.nasa.gov/)). The Doppler wind data taken from the UMBC wind lidar and are publicly available at ([https://www-](https://www-air.larc.nasa.gov/cgi-bin/ArcView/owlets.2018)
918 [air.larc.nasa.gov/cgi-bin/ArcView/owlets.2018](https://www-air.larc.nasa.gov/cgi-bin/ArcView/owlets.2018)). The GEOS-CF model simulation data were provided directly from the NASA
919 Center Global Modeling and Assimilation Office (GMAO) at the Goddard Space Flight Center
920 (https://gmao.gsfc.nasa.gov/weather_prediction/GEOS-CF/).

921 **References**

- 922 [Alonso, A. M., Berrendero, J. R., Hernández, A., and Justel, A.: Time Series Clustering Based on Forecast Densities,](#)
923 [Computational Statistics & Data Analysis, 51\(2\), 762–776., https://doi.org/10.1016/j.csda.2006.04.035, 2006.](#)
- 924 [Banta, R. M., Senff, C. J., Nielsen-Gammon, J., Darby, L. S., Ryerson, T. B., Alvarez, R. J., Sandberg, S. P., Williams, E. J.,](#)
925 [and Trainer, M: A bad air day in Houston. Bulletin of the American Meteorological Society, 86\(5\), 657–](#)
926 [670. https://doi.org/10.1175/BAMS-86-5-657, 2005.](#)
- 927 [Bernier, C., Wang, Y., Estes, M., Lei, R., Jia, B., Wang, S., and Sun, J.: Clustering Surface Ozone Diurnal Cycles to Understand](#)
928 [the Impact of Circulation Patterns in Houston, TX, Journal of Geophysical Research: Atmospheres, 124\(23\), 13457–](#)
929 [13474., https://doi.org/10.1029/2019jd031725, 2019.](#)
- 930 [Caicedo, V., Rappenglueck, B., Cuchiara, G., Flynn, J., Ferrare, R., Scarino, A. J., Berkoff, T., Senff, C., Langford, A., and](#)
931 [Lefer, B.: Bay Breeze and Sea Breeze Circulation Impacts on the Planetary Boundary Layer and Air Quality from an](#)
932 [Observed and Modeled Discover-AQ Texas Case Study, Journal of Geophysical Research: Atmospheres, 124\(13\),](#)
933 [7359-7378, https://doi.org/10.1029/2019jd030523, 2019.](#)
- 934 [Charrad, M., Ghazzali, N., Boiteau, V., and Niknafs, A.: NBCLUST: An R package for Determining the Relevant Number of](#)
935 [Clusters in a Data Set, Journal of Statistical Software, 61,\(6\), https://doi.org/10.18637/jss.v061.i06, 2014.](#)
- 936 [Christiansen, B.: Atmospheric Circulation Regimes: Can Cluster Analysis Provide the Number?, Journal of Climate, 20\(10\),](#)
937 [2229–2250., https://doi.org/10.1175/jcli4107.1, 2007.](#)

938 [Coggon, M. M., Gkatzelis, G. I., McDonald, B. C., Gilman, J. B., Schwantes, R. H., Abuhassan, N., Aikin, K. C., Arend, M.](#)
939 [F., Berkoff, T. A., and Brown, S. S.: Volatile chemical product emissions enhance ozone and modulate urban](#)
940 [chemistry, Proceedings of the National Academy of Sciences, 118,32, National Academy of Sciences,](#)
941 <https://doi.org/10.1073/pnas.2026653118>, 2021.

942 [Couillard, M. H., Schwab, M. J., Schwab, J. J., Lu, C. H., Joseph, E., Stutsrim, B., Shrestha, B., Zhang, J., Knepp, T. N., and](#)
943 [Gronoff, G. P., Vertical Profiles of Ozone Concentrations in the Lower Troposphere Downwind of New York City](#)
944 [during LISTOS 2018-2019, Journal of Geophysical Research: Atmospheres, 126\(23\), e2021JD035108,](#)
945 <https://doi.org/10.1029/2021JD035108>, 2021.

946 [Darby, L. S.: Cluster Analysis of Surface Winds in Houston, Texas, and the Impact of Wind Patterns on Ozone, Journal of](#)
947 [Applied Meteorology, 44\(12\), 1788–1806., https://doi.org/10.1175/jam2320.1, 2005.](#)

948 [Davis, R. E., Normile, C. P., Sitka, L., Hondula, D. M., Knight, D. B., Gawtry, S. P., and Stenger, P. J.: A Comparison of](#)
949 [Trajectory and Air Mass Approaches to Examine Ozone Variability, Atmospheric Environment, 44\(1\), 64–74.,](#)
950 <https://doi.org/10.1016/j.atmosenv.2009.09.038>, 2010.

951 [De Young, R., Carrion, W., Ganoe, R., Pliutau, D., Gronoff, G., Berkoff, T., and Kuang, S.: Langley Mobile Ozone LIDAR:](#)
952 [Ozone and Aerosol Atmospheric Profiling for Air Quality Research, Applied Optics, 56\(3\), 721,](#)
953 <https://doi.org/10.1364/ao.56.000721>, 2017.

954 [Dreessen, J., Orozco, D., Boyle, J., Szymborski, J., Lee, P., Flores, A., and Sakai, R. K.: Observed Ozone over the Chesapeake](#)
955 [Bay Land-Water Interface: The Hart-Miller Island Pilot Project, Journal of the Air & Waste Management Association,](#)
956 [69, \(11\), 1312–1330, https://doi.org/10.1080/10962247.2019.1668497, 2019.](#)

957 [EPA NEI \(National Emissions Inventory v1\): Air Pollutant Emission Trends Data, available at:](#)
958 <http://www.epa.gov/ttn/chief/trends/index.html> last access: 23 June 2015.

959 [Farris, B. M., Gronoff, G. P., Carrion, W., Knepp, T., Pippin, M., and Berkoff, T. A.: Demonstration of an off-Axis Parabolic](#)
960 [Receiver for near-Range Retrieval of Lidar Ozone Profiles, Atmospheric Measurement Techniques, 12\(1\), 363–370,](#)
961 <https://doi.org/10.5194/amt-12-363-2019>, 2019.

962 [Gelaro, R., Gelaro, R., McCarty, W., Suárez, M. J., Todling, R., Molod, A., Takacs, L., Randles, C. A., Darmenov, A.,](#)
963 [Bosilovich, M. G. Reichle, R., Wargan, K., Coy, L., Cullather, R., Draper, C., Akella, S., Buchard, V., Conaty, A., da](#)
964 [Silva, A. M., Gu, W., Kim, G-K., Koster, R., Lucchesi, R., Merkova, D., Nielsen, J. E., Partyka, G., Pawson, S., Putman,](#)
965 [W., Rienecker, M., Schubert, S. D., Sienkiewicz, M., and Zhao, B.: The Modern-Era Retrospective Analysis for Research](#)
966 [and Applications, Version 2 \(Merra-2\), Journal of Climate, 30\(14\), 5419–5454., https://doi.org/10.1175/jcli-d-16-0758.1,](#)
967 [2017.](#)

968 [Gronoff, G., Robinson, J., Berkoff, T., Swap, R., Farris, B., Schroeder, J., Halliday, H.S., Knepp, T., Spinei, E., Carrion,](#)
969 [W., Adcock, E.E., Johns, Z., Allen, D., Pippin, M.: A Method for Quantifying near Range Point Source Induced O3](#)
970 [Titration Events Using Co-Located Lidar and Pandora Measurements, Atmospheric Environment, 204, 43–52,](#)
971 <https://doi.org/10.1016/j.atmosenv.2019.01.052>, 2019

972 [Gronoff, G., Berkoff, T., Knowland, K.E., Lei, L., Shook, M., Fabbri, B., Carrion, W., Langford, A. O.: Case study of](#)
973 [stratospheric Intrusion above Hampton, Virginia: lidar-observation and modeling analysis, Atmospheric Environment,](#)
974 [259,118498, 1352-2310, <https://doi.org/10.1016/j.atmosenv.2021.118498>, 2021.](#)

975 [Han, J. and Kamber, M.: Data mining: concepts and techniques, San Francisco: Morgan Kaufmann Publishers, 2001.](#)

976 [Holmes, C. D., Bertram, T. H., Confer, K. L., Graham, K. A., Ronan, A. C., Wirks, C. K., and Shah, V.: The Role of Clouds](#)
977 [in the Tropospheric NO_x Cycle: A New Modeling Approach for Cloud Chemistry and Its Global Implications, Geophys.](#)
978 [Res. Lett., 46, 4980–4990, <https://doi.org/10.1029/2019GL081990>, 2019.](#)

979 [Hu, L., Keller, C. A., Long, M. S., Sherwen, T., Auer, B., Da Silva, A., Nielsen, J. E., Pawson, S., Thompson, M. A., Trayanov,](#)
980 [A. L., Travis, K. R., Grange, S. K., Evans, M. J., and Jacob, D. J.: Global simulation of tropospheric chemistry at 12.5 km](#)
981 [resolution: performance and evaluation of the GEOS-Chem chemical module \(v10-1\) within the NASA GEOS Earth](#)
982 [system model \(GEOS-5 ESM\), Geosci. Model Dev., 11, 4603–4620, <https://doi.org/10.5194/gmd-11-4603-2018>, 2018.](#)

983 [Kaufman, L. and Rousseeuw, P.: Finding groups in data: An introduction to cluster analysis, New York, Wiley, 1990.](#)

984 [Keller, C.A., Knowland, K.E., Duncan, B.N., Liu, J., Anderson, D.C., Das, S., Lucchesi, R.A., Lundgren, E.W., Nicely, J.M.,](#)
985 [Nielsen, E., Ott, L.E., Saunders, E., Strode, S.A., Wales, P.A., Jacob, D.J., and Pawson, S.: Description of the NASA](#)
986 [Geos Composition Forecast Modeling System GEOS-CF v1.0, Journal of Advances in Modeling Earth Systems, 13\(4\),](#)
987 [https://doi.org/10.1029/2020ms002413, 2021.](#)

988 [Knowland, K.E., Keller, C.A., Lucchesi, R.: File specification for GEOS-CF products, GMAO office note No. 17 \(version](#)
989 [1.0\). available from: \[https://gmao.gsfc.nasa.gov/pubs/office_notes.php\]\(https://gmao.gsfc.nasa.gov/pubs/office_notes.php\), 32, 2019.](#)

990 [Knowland, K. E., Keller, C. A., Wales, P. A., Wargan, K., Coy, L., Johnson, M. S., Liu, J., Lucchesi, R. A., Eastham, S. D.,](#)
991 [Fleming, E. L., Liang, Q., Leblanc, T., Livesey, N. J., Walker, K. A., Ott, L. E., and Pawson, S.: NASA GEOS](#)
992 [Composition Forecast Modeling System GEOS-CF v1.0: Stratospheric Composition, 14\(6\), e2021MS002852,](#)
993 [https://doi.org/10.1002/essoar.10508148.1, 2021.](#)

994 [Lawson, R. G., and Jurs, P. C.: New Index for Clustering Tendency and Its Application to Chemical Problems, Journal of](#)
995 [Chemical Information and Computer Sciences, 30\(1\), 36–41., <https://doi.org/10.1021/ci00065a010>, 1990.](#)

996 [Leblanc, T., Brewer, M. A., Wang, P. S., Granados-Muñoz, M. J., Strawbridge, K. B., Travis, M., Firanski, B., Sullivan, J. T.,](#)
997 [McGee, T. J., Sumnicht, G. K., Twigg, L. W., Berkoff, T. A., Carrion, W., Gronoff, G., Aknan, A., Chen, G., Alvarez,](#)
998 [R. J., Langford, A. O., Senff, C. J., Kirgis, G., Johnson, M. S., Kuang, S., and Newchurch, M. J.: Validation of the TOLNet](#)
999 [lidars: the Southern California Ozone Observation Project \(SCOOP\), Atmos. Meas. Tech., 11, 6137–6162,](#)
000 [https://doi.org/10.5194/amt-11-6137-2018, 2018.](#)

001 [Lei, L., Berkoff, T. A., Gronoff, G., Su, J., Nehrir, A. R., Wu, Y., Moshary, F., and Kuang, S.: Retrieval of UVB aerosol](#)
002 [extinction profiles from the ground-based Langley Mobile Ozone Lidar \(LMOL\) system, Atmos. Meas. Tech., 15, 2465–](#)
003 [2478, <https://doi.org/10.5194/amt-15-2465-2022>, 2022.](#)

004 [Li, W., Wang, Y., Bernier, C., and Estes, M.: Identification of Sea Breeze Recirculation and Its Effects on Ozone in Houston,](#)
005 [TX, during Discover-Aq 2013, Journal of Geophysical Research: Atmospheres, 125\(22\),](#)
006 <https://doi.org/10.1029/2020jd033165>, 2020.

007 [Little, R. J., A., and Rubin, D., B.: Statistical Analysis with Missing Data. Second ed., Wiley, 1987.](#)

008 [Mao, J., Zhao, T., Keller, C. A., Wang, X., McFarland, P. J., Jenkins, J. M., and Brune, W. H.: Global Impact of Lightning-](#)
009 [Produced Oxidants, Geophys. Res. Lett., 48, https://doi.org/10.1029/2021GL095740](#), 2021.

010 [McDuffie, E. E., Smith, S. J., O'Rourke, P., Tibrewal, K., Venkataraman, C., Marais, E. A., Zheng, B., Crippa, M., Brauer,](#)
011 [M., and Martin, R. V.: A global anthropogenic emission inventory of atmospheric pollutants from sector- and fuel-specific](#)
012 [sources \(1970–2017\): an application of the Community Emissions Data System \(CEDS\), Earth Syst. Sci. Data, 12, 3413–](#)
013 [3442, https://doi.org/10.5194/essd-12-3413-2020](https://doi.org/10.5194/essd-12-3413-2020), 2020.

014 [Orbe, C., Oman, L. D., Strahan, S. E., Waugh, D. W., Pawson, S., Takacs, L. L., and Molod, A. M.: Large-scale atmospheric](#)
015 [transport in GEOS replay simulations, J. Adv. Model. Earth Syst., 9, 2545–2560, https://doi.org/10.1002/2017MS001053,](#)
016 [2017.](#)

017 [Ring, A. M., Canty, T. P., Anderson, D. C., Vinciguerra, T. P., He, H., Goldberg, D. L., Ehrman, S. H., Dickerson, R. R., and](#)
018 [Salawitch, R. J.: Evaluating commercial marine emissions and their role in air quality policy using observations and the](#)
019 [CMAQ model, Atmospheric Environment, 173, 96-107, https://doi.org/10.1016/j.atmosenv.2017.10.037](#), 2018.

020 [Stauffer R.M., Thompson A.M., and Witte J.C.: Characterizing Global Ozonesonde Profile Variability from Surface to the](#)
021 [UT/LS with a Clustering Technique and MERRA-2 Reanalysis, J Geophys Res Atmos. 123\(11\):6213-6229,](#)
022 <https://doi.org/10.1029/2018JD028465>, 2018.

023 [Strode, S. A., Ziemke, J.R., Oman, L. D., Lamsal, L. N., Olsen, M. A., and Liu, J.: Global changes in the diurnal cycle of](#)
024 [surface ozone, Atmospheric Environment, 199, 323-333, https://doi.org/10.1016/j.atmosenv.2018.11.028](#), 2019.

025 [Sullivan, J. T., McGee, T. J., Leblanc, T., Sumnicht, G. K., and Twigg, L. W.: Optimization of the GSFC TROPOZ DIAL](#)
026 [retrieval using synthetic lidar returns and ozonesondes – Part 1: Algorithm validation, Atmos. Meas. Tech., 8, 4133–](#)
027 [4143, https://doi.org/10.5194/amt-8-4133-2015](https://doi.org/10.5194/amt-8-4133-2015), 2015.

028 [Sullivan, J.T., McGee, T.J., DeYoung, R., Twigg, L.W., Sumnicht, G.K., Pliutau, D., Knepp, T., and Carrion, W.: Results](#)
029 [from the NASA GSFC and LaRC Ozone Lidar intercomparison: new mobile tools for atmospheric research, J. Atmos.](#)
030 [Ocean. Technol., 32 \(10\), 1779-1795, https://doi.org/10.1175/JTECH-D-14-00193.1](#), 2015.

031 [Thompson, A. M., Stauffer, R. M., Miller, S. K., Martins, D. K., Joseph, E., Weinheimer, A. J., and Diskin, G. S.: Ozone](#)
032 [profiles in the Baltimore-Washington region \(2006-2011\): satellite comparisons and DISCOVER-AQ observations, J](#)
033 [Atmos Chem., 72\(3-4\), 393-422. https://doi.org/10.1007/s10874-014-9283-z](#), 2015.

034 [Torgo, L.: Data Mining with R, Chapman & Hall/CRC Data Mining and Knowledge Discovery Series,](#)
035 <https://doi.org/10.1201/b10328>, 2010.

036 [Wang, L., Newchurch, M. J., Alvarez, R. J., Berkoff, T. A., Brown, S. S., Carrion, W., De Young, R. J., Johnson, B. J., Ganoe,](#)
037 [R., Gronoff, G., Kirgis, G., Kuang, S., Langford, A. O., Leblanc, T., McDuffie, E. E., McGee, T. J., Pliutau, D., Senff,](#)

038 [C. J., Sullivan, J. T., Sumnicht, G., Twigg, L. W., and Weinheimer, A. J.: Quantifying TOLNet Ozone Lidar Accuracy](#)
039 [during the 2014 DISCOVER-AQ and FRAPPÉ Campaigns. Atmos Meas Tech, 10\(10\), 3865-3876,](#)
040 <http://doi.org/10.5194/amt-10-3865-2017>. 2017.

041 [Wang, X., Jacob, D. J., Downs, W., Zhai, S., Zhu, L., Shah, V., Holmes, C. D., Sherwen, T., Alexander, B., Evans, M. J.,](#)
042 [Eastham, S. D., Neuman, J. A., Veres, P. R., Koenig, T. K., Volkamer, R., Huey, L. G., Bannan, T. J., Percival, C. J.,](#)
043 [Lee, B. H., and Thornton, J. A.: Global tropospheric halogen \(Cl, Br, I\) chemistry and its impact on oxidants, Atmospheric](#)
044 [Chem. Phys., 21, 13973–13996, https://doi.org/10.5194/acp-21-13973-2021, 2021.](#)

045 [Wu, Y., Nehrir, A. R., Ren, X., Dickerson, R. R., Huang, J., Stratton, P. R., Gronoff, G., Kooi, S. A., Collins, J. E., and](#)
046 [Berkoff, T. A.: Synergistic aircraft and ground observations of transported wildfire smoke and its impact on air quality](#)
047 [in New York City during the summer 2018 LISTOS campaign, Science of The Total Environment, 773,145030,](#)
048 <https://doi.org/10.1016/j.scitotenv.2021.145030>, 2021.